



**POSITRON ANNIHILATION RATIO
SPECTROSCOPY STUDY OF
ELECTRIC FIELDS APPLIED TO
POSITRONIUM AT MATERIAL
INTERFACES**

THESIS

Ariella C. Walker, 2nd Lt, USAF

AFIT/GNE/ENP/11-M19

**DEPARTMENT OF THE AIR FORCE
AIR UNIVERSITY**

AIR FORCE INSTITUTE OF TECHNOLOGY

Wright-Patterson Air Force Base, Ohio

APPROVED FOR PUBLIC RELEASE; DISTRIBUTION UNLIMITED.

The views expressed in this thesis are those of the author and do not reflect the official policy or position of the United States Air Force, the Department of Defense, or the United States Government. This material is declared a work of the U.S. Government and is not subject to copyright protection in the United States.

AFIT/GNE/ENP/11-M19

POSITRON ANNIHILATION RATIO SPECTROSCOPY STUDY OF ELECTRIC FIELDS
APPLIED TO POSITRONIUM AT MATERIAL INTERFACES

THESIS

Presented to the Faculty

Department of Engineering Physics

Graduate School of Engineering and Management

Air Force Institute of Technology

Air University

Air Education and Training Command

In Partial Fulfillment of the Requirements for the

Degree of Master of Science

Ariella C. Walker, BS

2nd Lieutenant, USAF

March 2011

APPROVED FOR PUBLIC RELEASE; DISTRIBUTION UNLIMITED.

AFIT/GNE/ENP/11-M19

POSITRON ANNIHILATION RATIO SPECTROSCOPY STUDY OF ELECTRIC FIELDS
APPLIED TO POSITRONIUM AT MATERIAL INTERFACES

Ariella C. Walker, BS
2nd Lieutenant, USAF

Approved:

Larry W. Burggraf, PhD (Chairman)

Date

Lt Col Christopher S. Williams, PhD (Member)

Date

Maj Benjamin R. Kowash, PhD (Member)

Date

ABSTRACT

The purpose of this research was to develop a new code to analyze the data from AFIT's positron annihilation of radiation spectrometer, PsARS, system. The PsARS was used to analyze positronium formation at the surface of a capillary tube coated with gold. Using energy and geometry filters, the PsARS code determined the ratio of ortho-positronium to para-positronium. An electric field applied across the capillary tube wall forced positrons to move towards the gold surface of the capillary tube and prevent them from dropping into the Ore gap before they reach the surface. Inside the Ore gap, the positrons are more likely to form positronium. With the addition of the electric field, the positrons gain energy to overcome the loss of energy from scattering. Once at the surface, a secondary electric field applied from the capillary tube surface to the vacuum chamber wall polarized the positronium, increasing their lifetimes. The capability to force the positrons to gather on the gold surface of the capillary tube was demonstrated. In addition to the PsARS system, a positron annihilation lifetime spectroscopy, PALS, system was used to analyze the lifetimes of the positrons.

AFIT/GNE/ENP/11-M19

To my twin, mother, and father

Acknowledgements

I would like to express my sincere appreciation to my research advisor, Dr. Larry Burggraf who answered all of my endless questions and provided insight to help focus the direction of my research. I want to thank my committee members Lieutenant Colonel Christopher Williams and Major Benjamin Kowash for their assistance in helping me properly set up my equipment and debugging the electronics. Also, I want to thank Mr. Eric Taylor for helping me in my day to day activities in the laboratory and lending his expertise in trying to solve vacuum pressure problem, and Dr. Michael Lindsay for his expertise in developing the PALS system and sending me new updates to the code.

I am very grateful for First Lieutenant William Harrell in helping me set up and develop the MATLAB™ PALS system. I also would like to thank Mr. Brian Harcek for supervising the Na-22 deposition of the copper standard source and capillary tube.

I would also like to thank the Air Force Office of Scientific Research for their economic support of this research.

Ariella C. Walker

Table of Contents

	Page
Abstract	iv
Acknowledgements	vi
List of Figures	ix
List of Tables	xi
1. Introduction	1
1.1 Motivation	1
1.2 Previous Student Research and Objective of Current Research	4
2. Theory	10
3. Equipment	23
3.1 $3\gamma/2\gamma$ Detector	23
3.1.1 Detector Overview	23
3.1.2 Detector Calibration, Analysis Code, and Accidental Coincidence Correction	28
3.2 Lifetime Measurements	42
3.2.1 Igor Pro PALS system	42
3.2.2 MATLAB™ PALS system	45
3.3 The Capillary Tube	53
3.4 Copper Standard Source and $3\gamma/2\gamma$ Correction Factor	62
4. Results and Analysis	64
4.1 Accidental Coincidence Correction	64
4.2 $3\gamma/2\gamma$ Correction Factor	65
4.3 $3\gamma/2\gamma$ Ratio Results	67
4.4 PALS Analysis	75
4.5 Second Capillary Tube	78
4.6 Future Improvements	78
5. Conclusion	82
Appendix A. Schematic of NaI(Tl) Detector Ring	84
Appendix B. MATLAB™ $3\gamma/2\gamma$ Analysis Code	85
Appendix C. data_cal_stream.m File	89
Appendix D. cal_scan.m File	92

	Page
Appendix E. cal_func.m Function File.....	93
Appendix F. Stream_data_PALS.m File	95
Appendix G. PALS_meas.m File	98
Appendix H. PALS_func.m File	99
Appendix I. find_midrise_time.m File	101
Bibliography	102

List of Figures

Figure	Page
1. Diagram of the electrode biasing needed to produce the nested trap.....	3
2. Lifetime spectrum collected from the gold capillary tube using the AFIT PALS system	8
3. Pulse height spectra of three photon annihilation at varying angles from a Na-22 source	13
4. Decay scheme of Na-22.....	14
5. Positron energy spectrum from Na-22 beta decay	14
6. Comparison of the effects of positive and negative static and alternating electric fields on Ps formation at room temperature.....	22
7. Schematic of the AFIT ring detector made of six NaI(Tl) scintillation crystals.....	24
8. Picture of the AFIT NaI(Tl) ring detector	24
9. Diagram placement of the backplane connector on the 16 pin connector in a two module system	25
10. Example of an output file from the Igor Pro system using the energy and time only run type.....	27
11. Diagram of experimental setup to determine the best operating voltage of each PMT	28
12. Picture of the lead cave the vacuum chamber system was set up in.	29
13. Background spectrum collected using a BaF ₂ detector located outside of the lead cave.....	30
14. Background spectrum collected using a BaF ₂ detector located inside of the lead cave	30
15. Numbering system used to identify the PMT's when looking at the front of the NaI(Tl) detector	31
16. Holder developed by 2 nd Lt Robert Slaughter to allow calibration sources to be centered inside the detector	33
17. Uncalibrated energy spectrum for channel number 1, within module 1, from measuring a Na-22 source for fifteen minutes.	34
18. Diagram of the 120 degree 3 γ count filter	37
19. Diagram of the adjacent 3 γ count filter.	37
20. Diagram of the two hit 3 γ count filter	38
21. An example of where times within an event will not match up for the PsARS system.....	39

Figure	Page
22. Setup of the PALS BaF ₂ detectors with respect to the capillary tube.....	46
23. Diagram of how the electronics are connected together to conduct the PALS experiment.....	47
24. Unfiltered waveform pulse from measuring a Na-22 source.....	49
25. Filtered waveform pulse, from measuring a Na-22 source, using a Savitzky-Golay filter.....	50
26. Energy spectrum from measuring a Cs-137 source for three hours.....	51
27. Cut away diagram of the custom made capillary tubes showing each material and its thickness.....	54
28. Diagram of polyethylene ring designed to hold the capillary tube in the center of the vacuum chamber.....	55
29. Experimental setup of the PsARS system with the capillary tube inside the NaI(Tl) detector.....	56
30. Calculation of the electric field at the top of the gold surface on the capillary tube with varying voltages applied to the silver layer	57
31. Plot of surface roughness over a 2000 nm smooth region of the capillary tube gathered using an AFM.....	58
32. Calculation of the electric field at the top of the gold surface on the capillary tube with varying voltages applied to the gold layer	59
33. Diagram showing the location of where the inner and outer voltages are applied to the capillary tube.	60
34. Picture of the copper standard source used to calculate the $3\gamma/2\gamma$ correction factor	63
35. $3\gamma/2\gamma$ ratio results by applying a voltage bias on the inner silver layer of the capillary tube. The ground was established at the vacuum chamber wall	68
36. $3\gamma/2\gamma$ ratio results by applying a voltage bias on the inner silver layer of the capillary tube. The ground was established at the outer gold layer	71
37. Number of 2γ counts from the $3\gamma/2\gamma$ ratio experiment with the ground applied to the gold layer.	72
38. Number of 3γ counts from the $3\gamma/2\gamma$ ratio experiment with the ground applied to the gold layer.....	73
39. $3\gamma/2\gamma$ ratio results by applying a voltage bias on the inner silver layer and outer gold layer of the capillary tube.	74
40. Lifetime spectrum from measuring the second capillary tube, with a bias of 75 V added to the silver layer, for 42 hours	77

List of Tables

Table	Page
1. PsARS measurement of gold coated capillary tube at 1 atm and a vacuum level of less than 10^{-3} torr	6
2. Experimental values of the average lifetimes and intensities of the positron annihilation in polyethylene under various static electric field values	21
3. Setup of the jumpers on the two XIA cards to make the right card the master and left card the terminator	25
4. Operating bias for each NaI(Tl) PMT	31
5. 3 gamma/2 gamma experiment filter settings	32
6. 3 gamma/2 gamma experiment pulse shape analysis settings	32
7. Gain, offset, and Tau settings for the NaI(Tl) detector	33
8. Coefficients for each NaI(Tl) detector's calibration equation	35
9. Resolution of the NaI(Tl) detector crystals, for each channel, at 122 keV and 511 keV	35
10. Igor Pro PALS parameters for the BaF ₂ detectors	44
11. Operating biases of the two BaF ₂ detectors	45
12. MATLAB™ PALS parameters for the BaF ₂ detectors	48
13. 3γ and 2γ accidental coincidence counts for three different total measurement times of the capillary tube	65

POSITRON ANNIHILATION RATIO SPECTROSCOPY STUDY OF ELECTRIC FIELDS APPLIED TO POSITRONIUM AT MATERIAL INTERFACES

1. Introduction

1.1 Motivation

The study of positrons is important to the DOD because they are valued for their ability to characterize material defects without destroying the material. The lifetimes of positrons injected into a material are proportional to the size of the defects in the material. This allows a characterization of the material without destroying it because the positrons annihilate with the electrons in the material, leaving the material's atoms or molecules intact. This will be discussed in further detail in chapter two.

Furthermore, the positron's use as a possible energy source in space travel has lead to the development of positron confinement. Researching technology that is used to confine positrons is important because large volumes of positrons could be built up to be used as fuel for space travel or to create a gamma-ray source. If antimatter could be used as a practical energy source, it would revolutionize space travel. Per nucleon, nuclear fusion releases more energy than fission, but no process has been developed that doesn't consume more energy than it produces. After atoms undergo nuclear fission or fusion, they leave behind daughter products, decreasing the efficiency of the process. However,

with positrons, when they annihilate with electrons, 100% of their mass is converted into energy. Using positrons for space travel would increase the efficiency of the fuel.

The limiting factor in space travel is the consumption and storage of fuel and the fuel's energy density. For a mission to occur within a reasonable amount of time, the velocity of the craft needs to be high. The best fuels for achieving a high velocity must have a large energy density and specific impulse. Antimatter can produce energy densities that are three orders of magnitude larger than fusion or fission and ten orders of magnitude larger than chemical reactions [4]. In an anti-hydrogen engine, the annihilation of protons and anti-protons release pions; the pions then heat a propellant, increasing its specific impulse [6]. This will produce a specific impulse of one million seconds, while the specific impulse of a common chemical propellant, hydrazine, is only 220 seconds [6]. Besides an increase of specific impulse, antimatter fuels have larger energy densities, too. Chemical fuels have specific energies of on the order of 10^7 J/kg whereas the antimatter fuels are nine orders of magnitude larger [18]. Specifically, the energy density of antimatter is 9×10^{16} J/kg [18] while a conventional propellant, such as kerosene, has an energy density of 3.5×10^7 J/L [7]. Current fuels are inefficient and thus the majority of spacecraft payloads are used to store fuel to compensate for the fuel's inefficiency. If anti-matter was used, depending on its density, it would reduce either the weight or amount of fuel, allowing more room for equipment and for the craft to achieve higher velocities, potentially decreasing mission travel times.

Besides its use as a possible fuel for space travel, past research on antimatter propulsion has lead to the invention of the Penning trap that confines positrons. A Penning trap confines charged particles using a solenoidal magnetic field to confine the

particles in the radial direction and static electric fields to confine them in the longitudinal direction [4]. Once in the trap, the particles will cool by releasing synchrotron radiation. In an experiment conducted at CERN, they were able to trap one million anti-protons [4]. Furthermore, a variation of the Penning trap, the nested trap, can be used to store two oppositely charged particle groups that overlap in space. This eliminates the need of having separate containers for both particles, saving both space and money. A nested trap can be produced from five cylindrical electrodes that are biased in such a way as to produce an elongated potential well, see Figure 1 [18].

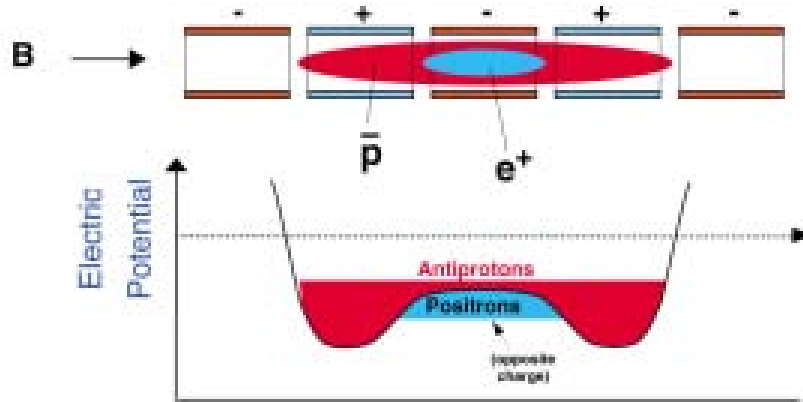


Figure 1. Diagram of the electrode biasing needed to produce the nested trap that confines both positrons and antiprotons. Each sequential horizontal electrode is biased opposite of the previous electrode.

Research on positron confinement is important because once large volumes of trapped positrons are created, the positrons can be used to create mono-energetic gamma-rays used for gamma-ray modulation. The gamma-ray laser would be created from a Bose Einstein condensates of positronium [23]. Current spectroscopic methods for studying different materials only gather information from using ultraviolet, visible, and infrared radiation. The only methods using gamma-rays come from positron angular correlation

annihilation radiation (ACAR) and Doppler broadening annihilation radiation (DBAR) measurements. ACAR measures the deviation from co-linearity of the two 511 keV annihilation photons in the laboratory frame of reference. DBAR measures the Doppler shift of the two 511 keV photons [24].

The gamma-rays are formed from the annihilation of electrons with positrons, commonly produced from radioactive beta decay. Positron confinement would reduce the need to rely solely on radioactive decay to garner gamma rays. Besides using electric and magnetic fields to confine the positrons, those fields can also be used to polarize a quasi-stable state the positron forms with an electron, positronium, increasing its lifetime.

Besides its possible future use as an energy source, the study of positrons is also valuable because they can be used to probe solids (metals, ionic solids, and molecular solids), liquids, and gases without destroying them. Scientists at Eglin AFB are developing a positron annihilation radiation spectroscopy (PAS) capability to characterize pore distributions in explosives [11]. Furthermore, PAS has previously been used to characterize defects in solid materials and semiconductors. This is possible because positronium, or Ps, most probabilistically only form in defects or gaps in solids with a periodic lattice structure and at the surface of materials. Based on the information gained from measuring the annihilation photons, the types, size, and locations of defects can be derived.

1.2 Previous Student Research and Objective of Current Research

The objective of this research is to understand how thermal Ps interacts with different materials and at different interfaces under the influence of an inhomogeneous electric

field. How the lifetime of the Ps and its decay mechanisms are influenced by external electric fields will also be studied. Ps likely forms at material surfaces, and by forcing the Ps to form at the surface, its interaction with the electric fields will be studied. This project is the continuation of a project started by Dr. Larry Burggraf and 2nd Lt Robert Slaughter from the previous year. Lt Slaughter developed a positron annihilation ratio spectroscopy (PsARS) code that determines the ratio to which Ps will annihilate via two or three photons. The second part of Lt Slaughter's work involved radioactive Na-22 deposited inside a capillary tube. The capillary tube was chosen for its ability to contain the Na-22 and moderate the positrons as they travel to the surface of the tube. The goal of this research is to discover how to maximize the amount of Ps formed at the surface of the capillary tube. Once at the surface, Ps annihilation can be altered through the use of applied electric fields. The positrons will be brought to the surface of the capillary tube by applying an electric field across the inner and outer wall of the capillary tube to keep the positrons from losing too much energy as they traverse through the capillary tube. Through the addition of an external electric field, the Ps may become polarized, altering the lifetime and decay mechanism of the Ps.

Lt Slaughter developed two methods to collect and analyze the $3\gamma/2\gamma$ data, the coincidence and non-coincidence methods. The non-coincidence method collects a spectrum from all segments from the detector and compares the energies of the photons to determine the number of two and three photon events. The counts in the 340 keV to 40 keV region are compared to the counts in the 511 keV peak. The counts are normalized to a calibrated standard spectrum, and count and energy factors are applied to calculate the $3\gamma/2\gamma$ ratio. In the coincidence method, developed at AFIT, the energy and

timing information from the different detector segments are used to employ a geometry filter to distinguish three photon counts from two photon counts. Four of the detector segments look for three photon events and the other two segments look for two photon events.

Each method has their advantages and disadvantages. The advantage of the non-coincidence method is that because the three photon counts lie in the Compton continuum for the 511 keV photons, the background is reduced when the number of three photon counts is determined. However, with no information on which segments of the detector recorded the three photon events, their numbers could be artificially increased from Compton scattering between adjacent segments. The advantage of the coincidence method is that with the geometry requirements, the chance that three photon events could result from Compton scatters is reduced, but with only four of the six detector segments looking for three photon events, the method is highly inefficient. By combining the two methods together, a new method will be created that combines the advantages of both the energy and geometry method. Using both the coincidence and non-coincidence methods, Lt Slaughter measured the following $3\gamma/2\gamma$ ratio [2:114]:

Table 1. PsARS measurement of gold coated capillary tube at 1 atm and a vacuum level of less than 10^{-3} torr.

Pressure	Coincidence $3\gamma/2\gamma$ (1/372)	Non-coincidence $3\gamma/2\gamma$ (1/372)
Vacuum	2.44	3.78
STP	2.92	3.85

These PsARS results showed that Ps was forming on the surface of the capillary tube. The large ratio difference between the two methods occurred because the coincidence

method requires an additional geometrical correction factor that was not applied. The absent correct factor would account for the capillary tubing not being centered inside the vacuum chamber. The non-coincidence method does not require the capture of all three gamma emissions thereby estimating the $3\gamma/2\gamma$ ratio better [2:114]. Requiring the capture of all three gamma-rays is not required because the method uses a sample with a known $3\gamma/2\gamma$ ratio to calibrate the method. The measurements at vacuum are lower than the measurements at STP because Ps interacts with the atoms and molecules in the air at the surface of the capillary tube. In addition to the $3\gamma/2\gamma$ ratio, lifetime measurements of the tube confirm that Ps is forming on the gold surface on the outside of the tube.

To measure the lifetimes of the Ps, Lt Slaughter used the positron annihilation lifetime spectroscopy (PALS) method. This method used two BaF₂ detectors to measure the gamma rays released from the capillary tube. The detectors were placed under the capillary tube, facing each other. The gamma-ray released when the Na-22 decays indicates the birth of the positron. When the positron annihilates with an electron, two 511 keV gamma-rays are produced. These gamma-rays indicate the loss of the positron. The difference between the two times equals the lifetime of the positron. Once a lifetime spectrum is collected, the data is analyzed using a program call PALSfit. The PALSfit program uses a least squares regression to find the lifetimes. This method will be discussed in further detail in chapter 3. Figure 2 shows the lifetime spectrum collected from measuring the capillary tube for one week [2:117].

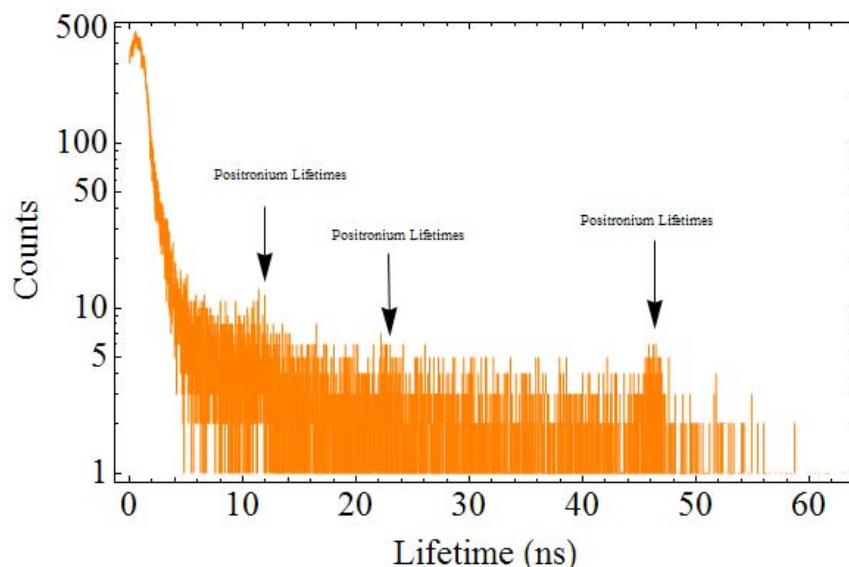


Figure 2. Lifetime spectrum collected from the gold capillary tube using the digital PALS system. The measurement lasted approximately one week [2:117].

This figure shows that several long lived Ps species exist, probably at the surface of the capillary tube. However, these peaks may also be the result of noise. Due to the significantly low number of counts, the PALSfit software was not able to find a best fit of the lifetime spectrum. To estimate the intensity of the predominate Ps term (47 nsec), the number of counts in the 47 nsec term is divided by the total number of counts and multiplied by their relative lifetimes. Lt Slaughter calculated the intensity of the 47 nsec lifetime to be approximately 8.5% [2:117].

Although many objectives were met by Lt Slaughter with his development of AFIT's PsARS code, numerous improvements can be made. When Lt Slaughter heated the capillary tubes to deposit the NaCl solution, much of the sodium leaked out. To decrease the amount that escapes, a possible improvement to the method would be to heat both ends of the tube, at a lower heat, and allow for the solution to evaporate over a longer period of time. Also, in the coincidence method, Lt Slaughter only used four

channels to record the three gamma spectrum. If all six were used, the measurement time would have been greatly reduced. Part of this research will involve configuring all six channels to communicate together. Lt Slaughter was forced to only use four channels to look for three photon events because the electronics were malfunctioning due to an unknown reason that prevented all six from communicating together. Furthermore, he only achieved a vacuum pressure of less than 10^{-3} torr, with the roughing pump. To use the ion pump, a starting pressure of less than 7.5×10^{-4} torr is needed. With the ion pump, pressures less than 10^{-12} torr will be achieved. At these lower pressures there are fewer atoms and molecules for the positrons to interact with at the surface of the capillary tube.

Positron research is important to the DOD because they can characterize materials without destroying the material. Furthermore, the size distribution of the defects can be calculated from analyzing the positron annihilation lifetime spectrum. In addition, research on positron confinement and lifetime extension will lead to the creation of gamma-ray lasers from Bose Einstein condensates of positronium. These, and further details of positron and positronium theory will be discussed in the next section.

2. Theory

The positron is the antiparticle of the electron. It has the same mass, spin, and charge as the electron, but is positively charged. In a vacuum, the particle is stable with a lifetime greater than 4×10^{23} years. However, when a positron travels through matter, it will annihilate having a lifetime that is inversely proportional to the local electron density [1:4]. Upon annihilation, the masses of the electron and positron are converted to energy which is released as gamma rays. The two most common numbers of gamma rays released are two and three. Higher numbers of gamma rays can be released, but are very improbable. Furthermore, a radiationless process of electron emission and a single gamma ray emission can occur, but because they can only occur in the presence of a nucleus to conserve energy, these events are very improbable. [1:4-6].

The most probable annihilation occurs when the spin of the two particles are anti-parallel, resulting in the singlet spin state. This process releases two gamma rays. The cross section of this reaction is

$$\sigma_{2\gamma} = \frac{4\pi r_o^2}{\gamma+1} \left[\frac{\gamma^2 + 4\gamma + 1}{\gamma^2 - 1} \ln(\gamma + \sqrt{\gamma^2 - 1}) - \frac{\gamma + 3}{\sqrt{\gamma^2 - 1}} \right] \quad [1:5] \quad (1)$$

where r_0 is the classical radius of the electron and γ is the Lorentz factor, which is calculated

$$\gamma = \frac{1}{\sqrt{1 - \beta^2}} \quad (2)$$

$$\text{where } \beta = \frac{v}{c} \quad (3)$$

with v equaling the speed of the positron and c equaling the speed of light in a vacuum [1:5]. In most situations, the positron is traveling at non-relativistic speeds, and the cross section equation reduces to

$$\sigma_{2\gamma} = \frac{4\pi r_o^2 c}{v} \quad [1:5]. \quad (4)$$

The rate at which the electron-positron pair decays into photons is referred to as the annihilation rate. It is calculated:

$$\lambda = \left\langle \psi \left| \sum_{e,p} \mathcal{K}_{e,p} \right| \psi \right\rangle \quad (5)$$

$$\mathcal{K}_{e,p} = 8\pi \sum_{S,M} D_S \left| \sigma_{S,M}(e,p) \right\rangle \delta^3(r_{ep}) \left\langle \sigma_{S,M}(e,p) \right| \quad (6)$$

where $\sigma_{S,M}$ is the annihilation cross section, ψ is the wave function of the electron and positron pair, r_{ep} is the average distance between the positron and electron, and D_S is a constant based on the spin [3:19]. In equation 5, the sum is over all electron-positron pairs in the system and in equation 6 the sum is where the spin, S , equals 0 and 1. Each D_S is calculated

$$\begin{aligned} D_0 &\approx 7.989 ns^{-1} \\ D_1 &\approx 7.040 \mu s^{-1} \quad [3:19]. \end{aligned} \quad (7)$$

When the total spin equals zero ($S=0$), the positron electron system is in the singlet state and when the spin equals one ($S=1$), the system is in the triplet state [3:19]. If the spins are anti-parallel, and the annihilation occurs when the positron has low energies, two annihilation photons are released, each with approximately 511 keV's of energy. In the laboratory reference frame, the photons are released almost 180 degrees

apart. In the center of mass frame, the photons are released exactly 180 degrees apart. If the spins of the electron and positron are parallel, three gamma rays are usually released [1:5,7]. When three photons are released, they can have a spectrum of energies from zero to 511 keV [25].

Whereas conservation of momentum and energy force two photon annihilations to have the same energy, released collinear, the extra degree of freedom in the three photon annihilation allow the photons to have a spectrum of energies and angular distributions [25]. In a triple coincidence experiment run by DeBenedetti and Siegel at the Carnegie Institute of Technology, the energy of the three 3γ photons were measured at varying angles. They used three NaI(Tl) scintillation detectors, 2.5 cm thick and 4 cm in diameter placed 12 cm from a Na-22 source [27]. Figure 3 shows the energies of the three photons at different angles from the source [reproduced from reference 27]. Also included is the case of two 511 keV photons as an energy reference for each detector.

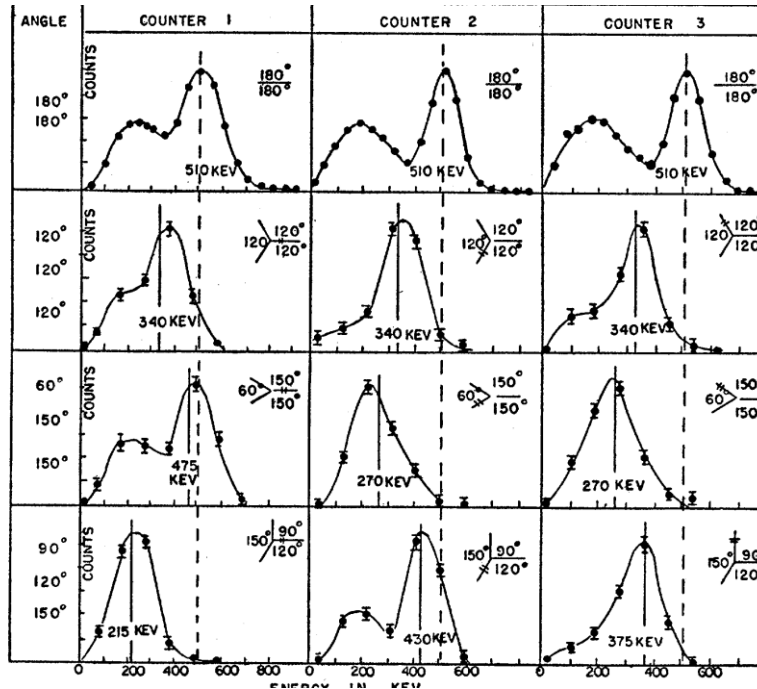


Figure 3. Pulse height spectra of three photon annihilation at varying angles from a Na-22 source [27].

With each NaI(Tl) detector located 120 degrees from the source, each photon is going to have an energy of 340 keV. As the angle between the detectors increase, as shown in the second case of 150 degrees, the photon takes away less energy, 270 keV, and the smallest angle, 60 degrees, took away the remaining 475 keV. However, every photon that is released at 120 degrees does not have 340 keV. As shown in the last case, each photon was released at a different angle, and all three had differing energies. The energy of a photon is dependent upon the angle at which the other two photons are released. Because there are essentially infinite combinations of angles with which the photons can be released, each photon can have a spectrum of energies from zero to 511 keV.

The most common source of positrons is when Na-22 undergoes beta plus decay. In beta plus decay, a proton is converted into a neutron and a positron and neutrino are

emitted. When Na-22 decays, 90.4% of the time it decays via β^+ to an excited state of Ne-22. 3.7 psec after the decay, a 1.274 MeV gamma ray is released. Figure 4 details the decay scheme and equation 8 shows the decay reaction [12:7].

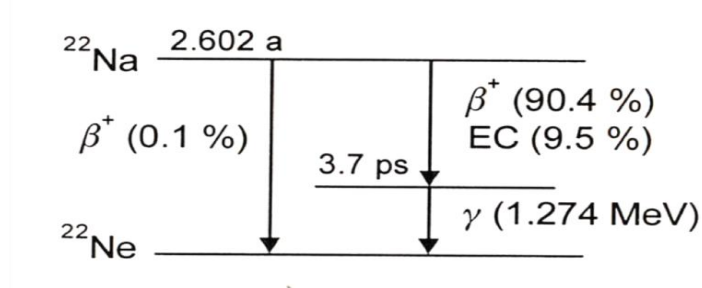


Figure 4. Decay scheme of Na-22 [12:7].



where γ is the gamma ray and ν is the neutrino. Due to the fact that the neutrino can be released with a spectrum of energies, the positron is also released with a spectrum of energies, see Figure 5 [2:6].

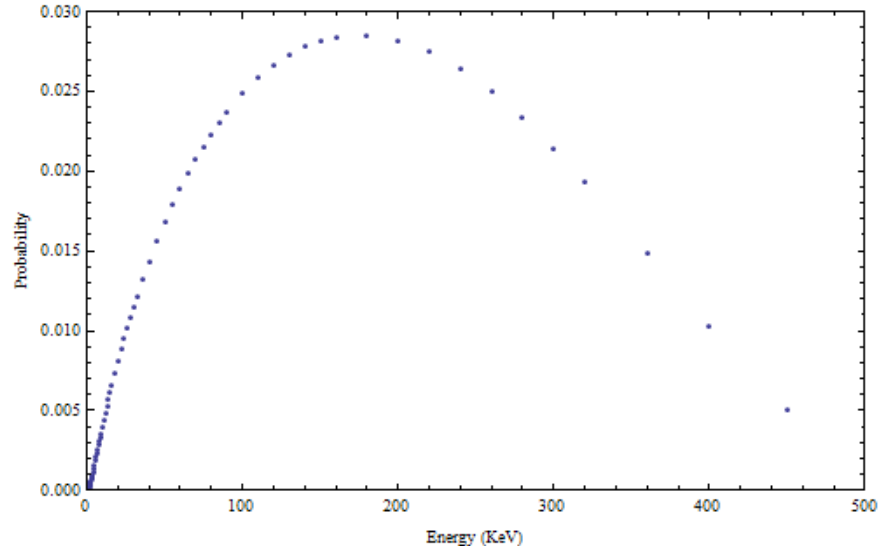


Figure 5. Positron energy spectrum from Na-22 beta decay [2:7].

Before annihilation occurs, the positron and electron can form a quasi-stable bound state, called positronium (Ps). Ps has a reduced mass that is half of the hydrogen atoms reduced mass. With a reduced mass that is half of hydrogen's, Ps has a ground state binding energy (6.8 eV) equal to half of hydrogen's ground state binding energy (13.6 eV). If the singlet state is formed, the Ps is called para-positronium (p-Ps), while the triplet state is called ortho-positronium (o-Ps). The number of gamma rays released for para and ortho is given by

$$(-1)^{n_\gamma} = (-1)^{L+S} \quad (9)$$

where S is the spin of the Ps, L is the orbital angular momentum of the Ps, and n_γ is the number of gamma rays released. In the ground state, p-Ps can only emit even numbers of gamma rays while o-Ps can only emit odd numbers of gamma rays. P-Ps mostly commonly emits two gamma rays while o-Ps mostly commonly emits three. Like free positron annihilation with an electron, higher numbers of gamma rays can be released, but these situations are very unlikely. The rate of ortho to para formation is 3:1. Therefore, three gamma annihilation is more abundant for Ps than for free positrons [1:7-8]. In a vacuum, Ps can only annihilate via three photons to conserve spin angular momentum [12:81].

The cross section ratio for three gamma to two gamma annihilation is 1/372 [14]. The ratio is calculated

$$\frac{\sigma_3}{\sigma_2} = \frac{3\tau_2}{\tau_3} \quad (10)$$

where σ_3 is the cross section of the o-Ps, σ_2 is the cross section of the p-Ps, τ_3 is the lifetime of the o-Ps, and τ_2 is the lifetime of the p-Ps. The factor of three is necessary

because o-Ps is three times more likely than p-Ps to form [26]. Given that the intrinsic lifetime of p-Ps is 0.125 ns and 142 ns for o-Ps, the cross section ratio is 0.00268, very close to the known 1/372 ratio [12:81].

In a gas, or at surfaces, Ps is formed when a hyper-thermal positron collides with an atom or molecule and takes away one of its electrons,



where X is the gas atom or molecule. For Ps to form,

$$E_{Ps} \geq E_i - \frac{6.8}{n_{Ps}^2} \quad (12)$$

where E_{Ps} is the energy of the positron, E_i is the ionization energy of the atom or molecule, and n_{Ps} is the principal quantum number, all numbers are in eV [1:27,151]. In a solid, Ps can form in defects in the material, in the natural voids in the material's matrix, or at material interfaces [1:27]. At material interfaces where the lattices do not match up, defects occur that act as positron traps [12:78]. Furthermore, the arrangement of the atoms in the material can create potential wells where the Ps can become trapped [1:27].

Inside pure, single crystal metals, Ps cannot form and persist due to the high density of the electrons, but can form at the surface of the metal [8]. As the positron approaches the surface, it can reflect back due to the surface potential barrier, escape as a positron, escape as Ps, or become trapped at a surface state. If the positron work function is positive and the Ps work function is negative, the positron will capture an electron and escape as Ps [8]. The Ps will have a kinetic energy less than or equal to the negative value

of the Ps formation potential, ϵ_{Ps} . The formation potential, in eV's, can be calculated from:

$$\epsilon_{Ps} = \varphi_+ + \varphi_- - \frac{6.8}{n_{Ps}^2} \quad (13)$$

where φ_+ and φ_- are the positron and electron work functions, respectively [1:27]. For ground state Ps, in most metals, the formation potential is negative, allowing for Ps to leave the surface. For most cases, the Ps will be in the ground state, $n_{Ps}=1$, and the binding energy of the Ps will be 6.8 eV [1:27].

If the work function of the positron is negative, the positron will accelerate toward the barrier and if it has enough energy, it can escape from the material. However, positron emission is suppressed as the temperature decreases, with no emission as the temperature reaches zero Kelvin [8]. A negative positron work function allows for spontaneous positron emission from the surface [8]. A negative work function is defined as the energy of the positron which has been thermalized as it travels through the material [9]. This means that the positron will leave the material with a minimum amount of kinetic energy [28].

Gold is one material with a negative positron work function [9]. In this experiment, because the capillary tube is coated with gold, it is expected most of the positrons ejected from the surface will possess an energy equal to the positron work function of gold, approximately negative 1 eV [9]. However, this only applies if the gold surface is clean. In this experiment, the gold surface is coated with multiple layers of hydrocarbons and moisture that build up from exposure to air. These hydrocarbon layers will have an effect on Ps formation and annihilation, altering the experimental results.

The study of negative work function materials is important because mono-energetic positron beams can be created from them. Further studies can be conducted by coating the gold with another material and the positrons emitted at the gold boundary layer can be used to investigate the defect characteristics of the added material. In addition to studying interactions in another material, a secondary applied potential between the vacuum tube and capillary tube intends to be used to suppress the positron emission or polarize the Ps on the gold surface to influence lifetimes.

Positrons are commonly formed through beta plus decay, with energies of several hundred keV. Once the positron is formed, it will lose energy through scattering. Although rare, a positron can lose half of its energy in a single head-on collision with a molecule or atom in the material the positron is traveling through [3:117-118]. Most scatters, though, are glancing collisions, resulting in an average energy loss of 30-50 eV per collision, with a maximum of 100 eV [3:117-118]. The positron will most likely form Ps if its energy, W , lies within the Ore gap. The Ore gap is defined as the energy interval

$$I_G - \frac{R_y}{2} < W < W_{ex} \quad (14)$$

or

$$I_G - \frac{R_y}{2} < W < I_G \quad (15)$$

where I_G is the first ionization potential of the molecule, $R_y/2$ is the binding energy of Ps in a vacuum, and W_{ex} is the electronic excitation threshold of the molecule. When the energy of the positron falls below the Ore gap, it does not have enough energy to ionize

the molecule and free an electron to form Ps. If the energy of the positron exceeds the Ore gap level, ionizations and electronic excitations will dominate, but Ps formation is still possible [3:123].

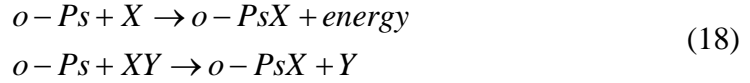
The rate at which Ps annihilates is called the annihilation rate and is influenced by the defects and pores inside the material, and through quenching. Quenching is the process through which o-Ps is transformed into p-Ps [3:3]. With quenching, the annihilation lifetimes decrease because the longer-lived o-Ps lifetimes are replaced with the shorter-lived p-Ps lifetimes. The annihilation rate of the Ps is dependent on the size of the trap. Assuming the trap is spherical, with a radius R , the annihilation rate for o-Ps is

$$\lambda_3(ns^{-1}) = 2\left[1 - \frac{R}{R_0} + \left(\frac{1}{2\pi}\right)\sin\left(\frac{2\pi R}{R_0}\right)\right] \quad (16)$$

where

$$R_0(nm) = R + .166 \quad (17)$$

for ionic and molecular solids [3:90-91]. In polymers, the p-Ps will decay quickly when the positron annihilates with its paired electron, also known as self annihilation. The longer-lived o-Ps can decay with its paired electron or via the pick off method, where the positron decays with an electron from a neighboring atom or molecule [3:3]. In addition, a second process called exchange quenching can occur. This is where the o-Ps exchanges its paired electron with an electron from a nearby atom or molecule, and transforms into p-Ps, where it will quickly decay. A third process, called chemical quenching, occurs when the o-Ps undergoes a chemical conversion. Two such examples are:



where X and Y are atoms or molecules [1:328-329]. All of these processes will shorten the o-Ps lifetime from 142 ns to a few ns [3:3]. Through the application of positron annihilation lifetime spectroscopy (PALS) on a material, the o-Ps lifetime can be determined and using equation 16, the size of the defects in the material can be characterized.

PALS can be used to measure both the size and concentration of defects in a material. The longer lifetime components of a PALS spectrum are due to a decrease in the local electron density. The strength of the longer lived component, or intensity, is related to the concentration of the defects in the material [19]. Lifetime measurements are commonly conducted by measuring a positron source, Na-22. The source is placed directly between the two detectors used to conduct the measurements. Detectors with fast timing components are needed to be able to resolve small time resolutions. Because the 1.274 Mev gamma ray from the Na-22 is released almost simultaneously with the positron, it indicates the birth of the positron. The time for the positron to thermalize, a few picoseconds, is so small compared to the lifetime of the positron that it can be neglected [19]. Once thermalized, the positron diffuses through the material before it is trapped. The diffusion length determines how many atoms the positron can probe for defects before it annihilates [19]. The diffusion length is thus an indication of how well the positron can probe the material for defects. When the positron annihilates, the annihilation photon indicates the positron's death. The difference between the two times

at which the birth gamma and annihilation photon are detected equal the lifetime of the positron [19].

When using PALS to determine the lifetimes of the positrons, the source activity must be low. If the activity is too high, more than one positron will be present in the material at the same time and the start and stop signals could be mixed up. However, if the source activity is too low, the measurement will take longer to collect [19]. To produce a complete spectrum, one million counts are needed.

Annihilation rates can be altered through the use of external electric or magnetic fields. Applying an external magnetic field to the Ps will cause the magnetic subset of the ortho and para-positronium to mix, increasing the lifetime of the p-Ps and decreasing the lifetime of o-Ps [3:91]. An experiment conducted by Stevens and Lichtenberger at the University of Guelph, Ontario, Canada, showed that the lifetimes of positrons annihilating in polyethylene were extended through the use of electric fields [16]. The experimental setup consisted of the Na-22 sandwiched between two nickel foils. Each layer on the foil was followed by a layer of polyethylene and then a layer of brass. Varying high voltages were applied to the brass layers to produce static electric field across the polyethylene [16]. Table 2 shows the results [reproduced from reference 16].

Table 2. Experimental values of the average lifetimes and intensities of the positron annihilation in polyethylene under various static electric field values [16].

E (kV/cm)	I_1 (%)	I_2 (%)	I_3 (%)	I_4 (%)	τ_1 (nsec)	τ_2 (nsec)	τ_3 (nsec)	τ_4 (nsec)
0	23.5	46.6	10.6	19.3	0.145	0.352	0.663	2.39
30	19.1	49.8	11.6	19.5	0.147	0.349	0.660	2.39
60	18.3	50.8	11.4	19.5	0.145	0.348	0.651	2.39
90	17.4	52.4	11.7	18.5	0.144	0.345	0.640	2.38
100	16.4	51.6	13.4	18.6	0.145	0.343	0.629	2.37
110	14.3	52.2	14.6	18.8	0.144	0.335	0.600	2.34
120	13.9	51.1	16.6	18.5	0.144	0.327	0.583	2.34

The results show that Ps can be polarized with an electric field of a magnitude less than 120 kV/cm [16].

Besides lifetimes, the intensity of the Ps can be influenced by electric fields. In an experiment run by Yasuo Ito at the Research Center for Nuclear Science and Technology at the University of Tokyo, Na-22 was deposited inside an envelope of nickel foils, which was then sandwiched between two low density polyethylene sample sheets. By applying a bias across the foils, the o-Ps intensity not only decreased as the electric field strength increased, but the polarity of the field did not significantly affect the intensity, as shown in Figure 6 [reproduced from reference 5]. In this experiment, the o-Ps intensity is a measure of the cross section for o-Ps formation. As the electric field strength increases, the field imparts more energy to the positron and when it ionizes an atom or molecule, the positron gives more energy to the electron. As the energy of the electron increases, the electron is more likely to escape before the positron can capture it and form o-Ps.

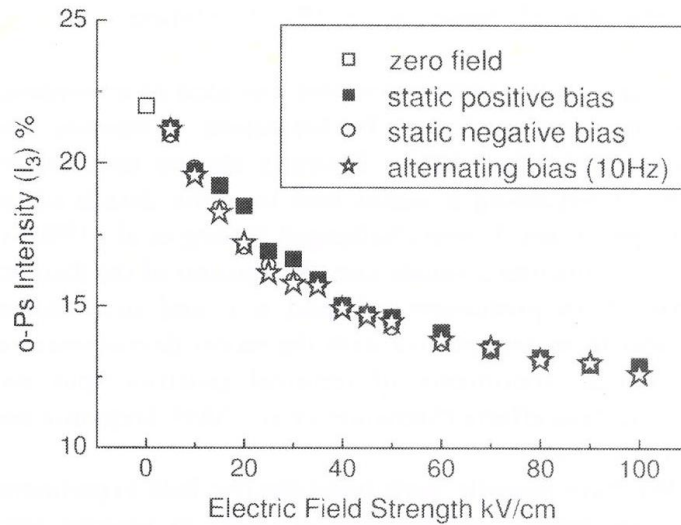


Figure 6. Comparison of the effects of positive and negative static and alternating electric fields on Ps formation at room temperature.

3. Equipment

The two aspects of this research involve conducting PsARS and PALS measurements. Each system has different requirements for its equipment due to the particular aspect of the positron annihilation that the system is measuring. For the PsARS system, the important factor is being able to capture the maximum amount of photons from the source. In PALS, the system must be able to resolve the time difference between the positron's birth and death photons. These different necessities lead to having separate detectors for each system.

3.1 $3\gamma/2\gamma$ Detector

3.1.1 Detector Overview

To measure the $3\gamma/2\gamma$ ratio, a positron annihilation of radiation spectroscopy, or PsARS, system is used. The digital PsARS system at AFIT consists of a thallium-doped NaI scintillation ring that is 18 cm long, has a 20 cm diameter, and a thickness of 3.5 cm. Figure 7 shows the location of the crystals within the ring, and Figure 8 shows a picture of the detector. The full detector schematic is attached in Appendix A. The six NaI(Tl) crystals were connected to six photomultiplier tubes, or PMTs. The PMT's are each connected to an ORTEC model 113 pre-amplifier. Each pre-amp is connected to an input channel in an XIA DGF4C revision E digital system, to convert the current pulses into digital data. Two cards are used because each card can only hold four channels. The signals are digitized using a 12 bit ADC at a rate of 500 MHz [17]. The XIA cards are controlled by a Weiner CC32 CAMAC controller. The signal from the controller is sent

to a computer, where it was analyzed using Igor Pro, a data analysis, image processing, and programming software tool.

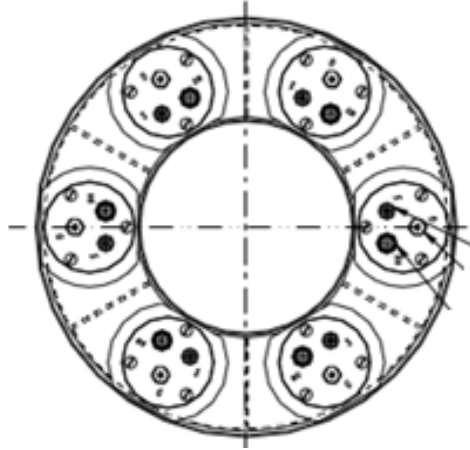


Figure 7. Schematic of the AFIT ring detector made of six NaI(Tl) scintillation crystals. Each crystal is optically separated from each other and connected to its own PMT.



Figure 8. Picture of the AFIT NaI(Tl) ring detector.

The right XIA card was set as the master card and the left card was set as the terminator card. Table 3 shows the configuration of the jumpers on the cards to achieve this setup.

Table 3. Setup of the jumpers on the two XIA cards to make the right card the master and left card the terminator

	Right card (s/n: 1230)	Left card (s/n: 1240)
Jumper 1	Attached	Detached
Jumper 2	Attached	Detached
Jumper 3	Detached	Attached
Jumper 4	Detached	Attached
Jumper 5	Board clock	External

In addition to the five jumpers listed above, all the jumpers to control the input impedances were set to 50 Ohms. To allow the two cards to communicate to each other, the backplane connector was connected to the row A of the 16 pin connector on each card, as shown in Figure 9.

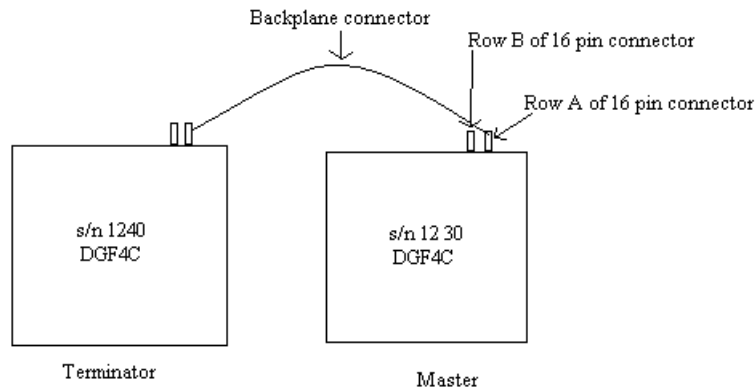


Figure 9. Diagram placement of the backplane connector on the 16 pin connector in a two module system.

Furthermore, a logic unit was added to the system so that when one module triggered, it forced the other module to trigger as well. This was accomplished by connecting the

busy-out signal of the DGF4C cards to the input of a Phillips Scientific model 757 mixed logic fan-in/fan-out unit and the output of the logic unit to the sync-in port on the DGF4C cards. To force both modules to trigger on any event, the coincidence pattern was set to include all possible coincidence configurations. This was accomplished using the settings tab of the DGF viewer (all boxes were selected including the “0000” pattern). The coincidence window was set to 50 ns, also located in the coincidence pattern function. With these settings, when any one of the six PMT’s registers a hit, it sends out a signal to the logic unit, and the logic unit forces all six PMT’s to collect a measurement for 50 ns.

A spectrum is collected from the run tab of the DGF viewer. The user can control the number of spills, polling time, and run time. A spill is when the DGF4C cards transfer their data to the computer. The cards can hold 256 kB of list mode data before its buffer is full and its memory is transferred to the computer [21]. The polling time is the time between each measurement. The run time is how long the data is collected for. The number of spills was set high enough to allow the run time to decrement to zero before the spills reached zero. The polling time was set to 0.05 μ sec. At the top of the tab is a drop down menu with different types of collection methods. The run type chosen was the “energy and time only” method. This method was chosen because its output file gives the channel number, energy, and trigger time for every event detected. Furthermore, the energy and time only aspect eliminates excess data in the output that would increase the file size. The output data is organized into columns. The first column contains the event number, the second column contains the channel number of the XIA signal, the third column contains the energy of the event (represented as channel number of the spectra),

and the fourth column identifies the time of the event. All of the events for module one are located in the top half of the file, while the events for module two are located in the bottom half of the file. Figure 10 shows an excerpt from an example output file.

Module: 1						
Run Task: 259						
Run Start Time: 0.001634						
Event No	Channel No	Energy	Trigger Time	XIA_PSA	User_PSA	
1	0	0	16336			
1	1	0	16336			
1	2	0	16336			
1	3	0	16336			
2	0	0	36911			
2	1	0	36911			
2	2	0	36911			
2	3	0	36911			
3	0	0	3275			
3	1	0	3275			
3	2	0	3275			
3	3	0	3275			
4	0	0	11104			
4	1	0	11104			
4	2	0	11104			
4	3	0	11104			
5	0	0	19333			
5	1	22382	19333			
5	2	3495	19333			
5	3	0	19333			
6	0	0	51178			
6	1	0	51178			
6	2	3778	51178			
6	3	0	51178			
7	0	0	47619			
7	1	0	47619			
7	2	0	47619			
7	3	0	47619			
8	0	0	27938			
8	1	0	27938			
8	2	28466	27938			
8	3	0	27938			
9	0	0	22325			
9	1	38315	22325			
9	2	35158	22325			
9	3	0	22325			
10	0	0	33794			

Figure 10. Example of an output file from the Igor Pro system using the energy and time only run type.

As can be seen from the figure, there is header data at the top of the file that identifies the module and run start time of the experiment. The run start time does not report what time the experiment started, but whether the two modules are synchronized at the start of the experiment. If the two modules are synced at the start of the data collection, the two run start times will read 0.001634. This same information exists in the middle of the file at

the start of module two's data. For the $3\gamma/2\gamma$ code to work properly, this information must be removed from the output file.

3.1.2 Detector Calibration, Analysis Code, and Accidental Coincidence Correction

The first step in calibrating the equipment involved determining the optimal operating voltage for each PMT. The electronics used were an ORTEC model 142 pre-amplifier, ORTEC model 556 high voltage (HV) power supply, ORTEC model 671 linear amplifier, ORTEC model 551 single channel analyzer (SCA), and an ORTEC model 996 counter. Figure 11 shows the experimental setup.

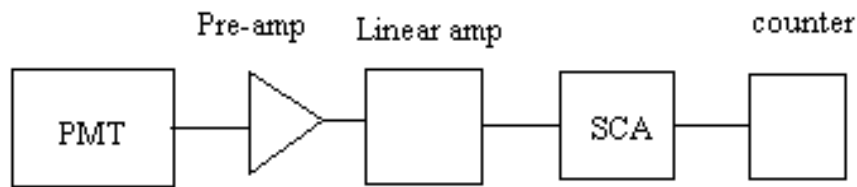


Figure 11. Diagram of experimental setup to determine the best operating voltage of each PMT

A Sr-85 source was measured because its 514 keV gamma ray is close to that of the 511 keV Ps annihilation photo and its activity was higher. To ensure the SCA triggered on the 514 keV gamma ray, a Tektronix TDS5104B digital phosphor oscilloscope was used to set the correct cut-off voltage. To minimize the background radiation, the NaI(Tl) detector and subsequent experiment was placed inside a lead cave, reference Figure 12. Figure 13 and 14 show background spectra collected outside and inside the lead cave, using a BaF₂ detector. Each measurement lasted 60 minutes. Comparing the two spectra, the lead cave suppressed the low energy background

radiation. Both figures show a high energy peak at a trigger voltage of approximately 0.2 V. However, this peak is a result of how the spectra are analyzed. All of the high energy gamma rays are grouped together in this one bin, making the appearance of high energy background source existing. An initial voltage of 500 V was applied to the PMT, and the counter recorded the number of counts in 10 sec. The voltage was incremented until the number of counts reached a peak. The operating voltage of each PMT is listed in Table 4. When looking at the NaI(Tl) detector from the front, PMT 1 is located at the top and the numbering system continues clockwise, reference Figure 15.

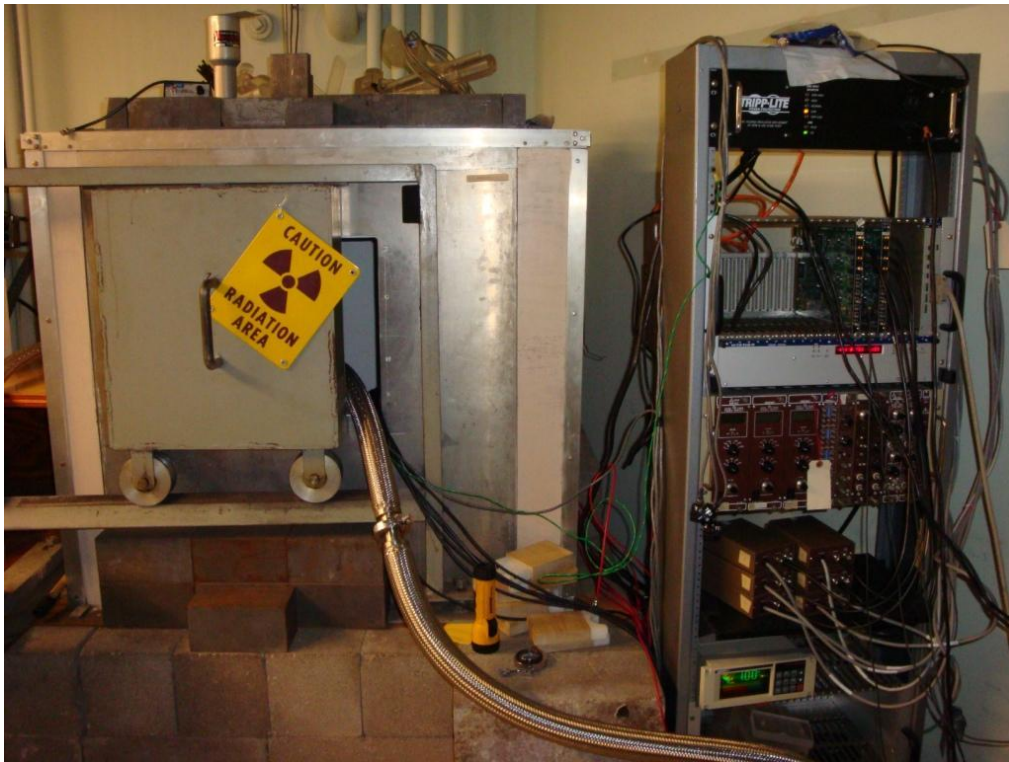


Figure 12. Picture of the lead cave the vacuum chamber system was set up in. Next to the lead cave is the crate containing the power suppliers, pre-amplifiers, CAMAC crate, XIA cards, and vacuum sensor display.

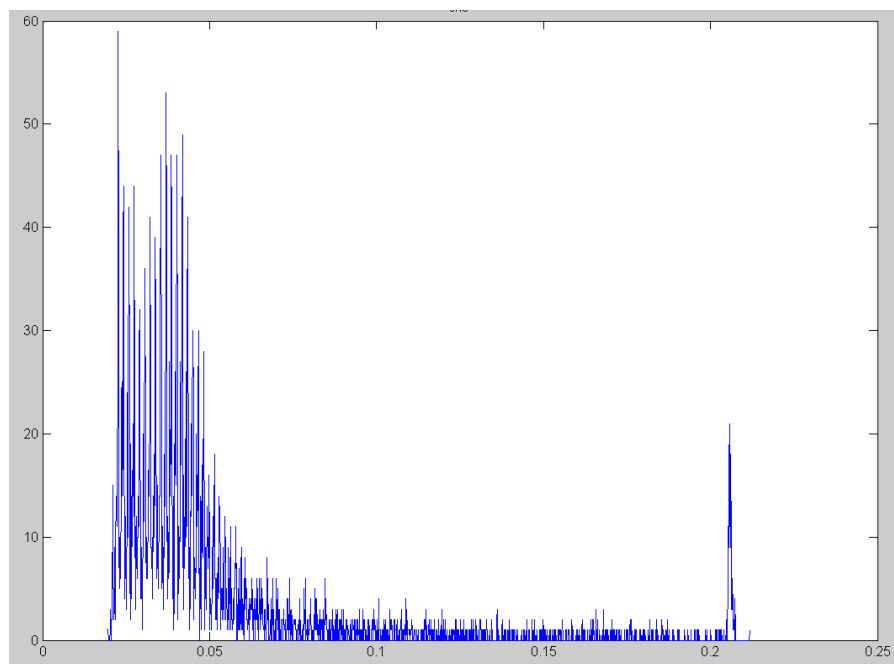


Figure 13. Background spectrum collected using a BaF₂ detector located outside of the lead cave. The measurement lasted 60 minutes.

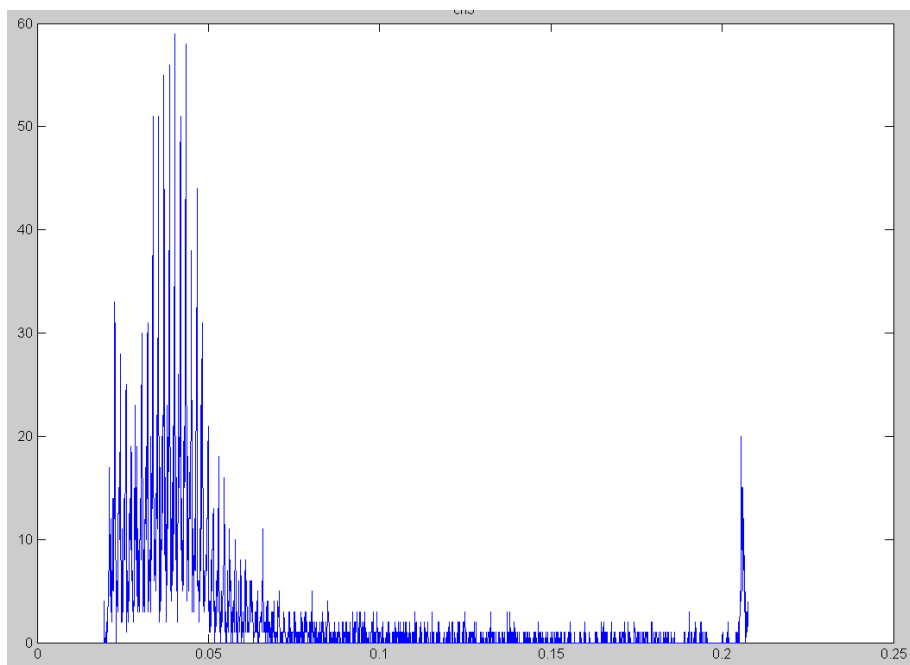


Figure 14. Background spectrum collected using a BaF₂ detector located inside of the lead cave. The measurement lasted 60 minutes.

Table 4. Operating bias for each NaI(Tl) PMT

PMT	Bias (V)
1	858
2	836
3	900
4	963
5	935
6	890

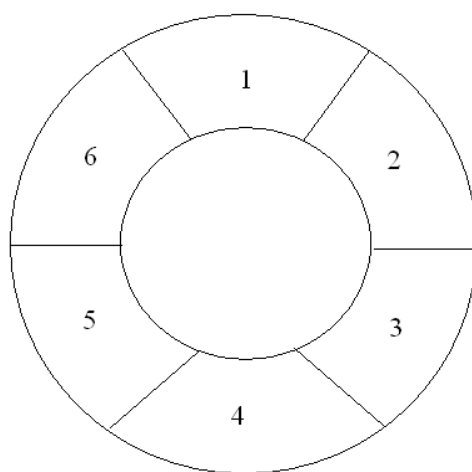


Figure 15. Numbering system used to identify the PMT's when looking at the front of the NaI(Tl) detector.

Due to the fact that only three dual power supplies were available to power the six PMT's, the PMT's had to be paired up based on similar operating voltages. PMT 1 and 2 were paired and used 831 V, PMT 3 and 6 were paired and used 890 V, and PMT 4 and 5 were paired and used 930 V. The bias chosen for each pair could not be an average and had to be the lower of the two optimal biases. Once the bias on the PMT increased past its optimal value, the count rate decreased. The rest of the calibration settings were determined using the Igor Pro GUI.

The filter and pulse shape analysis settings were chosen in order to minimize the full width at half maximum, FWHM, and thus minimize the detector resolution. These

parameters were optimized by 2nd Lt Robert Slaughter the previous year in his thesis experiment. Table 5 and 6 contain the values taken from his thesis:

Table 5. 3 gamma/2 gamma experiment filter settings [2:120]

	Trigger filter	Energy filter
Rise time (μ s)	0.1	2.8
Flat top (μ s)	0.1	1.2
Threshold	40	N/A

Table 6. 3 gamma/2 gamma experiment pulse shape analysis settings [2:120]

Trace length (μ s)	5
Delay (μ s)	2
PSA start (μ s)	0.025
PSA end (μ s)	4.975

The remaining parameters were determined using the built in functions from the DGF viewer. The gains for all the channels were adjusted so that full 1.274 MeV gamma ray peak could be seen on the DGF viewer's oscilloscope. If the gain was set too high, the peak of the 1.274 MeV gamma ray would be cut off and the signal would saturate the electronics. The offset values were also determined using the oscilloscope function. The offsets were first set using the "adjust offset function", but manually adjusted for better results. The decay times of the signals were set manually using the "manual Tau finder" DGF viewer function. The decay times had to be set individually to account for the slight differences between each PMT. Table 7 shows the gain, offset, and Tau settings for each of the channels. Lastly, on the run tab of the interface, the "simultaneously start/stop modules", "synchronize clocks", and "in every new run" boxes were checked to ensure the modules were synchronized and the polling time was set to 0.05 sec.

Table 7. Gain, offset, and Tau settings for the NaI(Tl) detector

	Gain (V/V)	Offset (V)	Tau (μ s)
Mod 1 ch 1	0.1640	1.0000	68.1501
Mod 1 ch 2	0.1640	1.0000	64.7665
Mod 2 ch 0	0.1640	1.0348	67.4105
Mod 2 ch 1	0.1640	1.0590	63.8633
Mod 2 ch 2	0.1640	1.0552	74.6553
Mod 2 ch 3	0.1640	1.0301	66.7308

The next step of calibration involved collecting spectra from different isotopes to create a calibration curve relating the channel number to the energy. Four radionuclides were measured: Co-57, Cs-137, Na-22, and Sr-85. Their respective gamma ray energies are: 122 keV, 662 keV, 511 keV, and 514 keV. These sources were chosen to ensure the calibration equation had a low, medium, and high energy data point. Each source was placed on a holder developed, by 2nd Lt Robert Slaughter, to ensure the source was centered inside the detector, reference Figure 16.



Figure 16. Holder developed by 2nd Lt Robert Slaughter to allow calibration sources to be centered inside the detector.

Each source was measured for 15 minutes to collect an energy spectra. Figure 17 shows the Na-22 energy spectrum for channel 1 of module 1, segment number 1 from the NaI(Tl) detector. The Igor pro program allows the user to be able to zoom in on the full energy peak, FEP, to pick out its location. These spectra were used to create the six energy calibration equations.

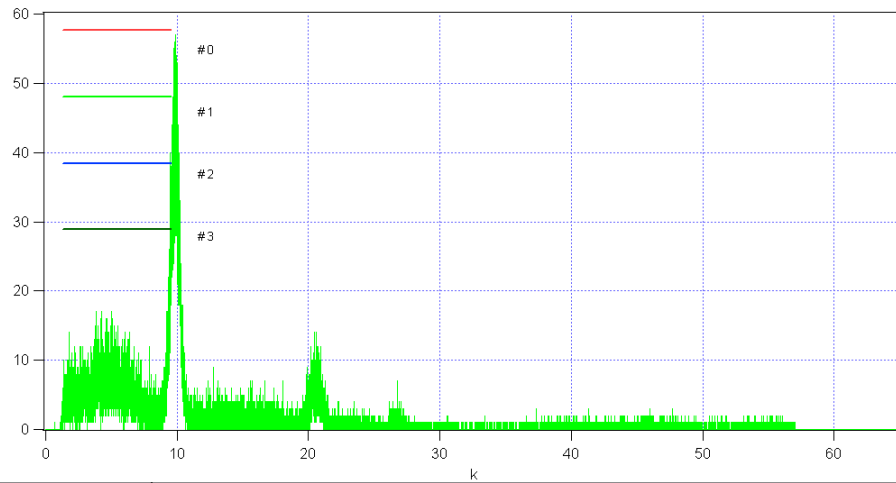


Figure 17. Uncalibrated energy spectrum for channel number 1, within module 1, from measuring a Na-22 source for fifteen minutes.

Given the location of each FEP for the four isotopes and all six channels, six calibration equations were determined. The calibration equations were determined using a best fit second order polynomial equation. The calibration coefficients and R-squared value for each equation are located in Table 8. R-squared is a measure of how close the best fit equation fits the data. The closer the value is to 1, the better the fit is. The coefficients take follow the format of:

$$Ax^2 + Bx + C \quad [15:442] \quad (19)$$

Table 8. Coefficients for each NaI(Tl) detector's calibration equation

	A	B	C	R ²
Mod 1 ch 1	-1.27325E-6	6.95083E-2	-6.57573E1	9.99984E-1
Mod 1 ch 2	6.82893E-7	1.95708E-2	1.62295E1	9.99994E-1
Mod 2 ch 0	-9.42006E-7	6.32250E-2	-6.03483E1	9.99973E-1
Mod 2 ch 1	-1.07175E-6	6.32157E-2	-6.79067E1	9.99996E-1
Mod 2 ch 2	1.63403E-7	1.89323E-2	2.38484E1	9.99974E-1
Mod 2 ch 3	-6.91681E-7	4.99622E-2	-6.32222E1	9.99999E-1

These spectra can also be used to determine the resolution of the detector. The resolution is a measure of how close in energy two gamma rays can be and also be resolved. Resolution is reported as a percentage, and smaller values are better than larger values. Resolution, R, is calculated:

$$R = \frac{FWHM}{H_o} \quad (20)$$

where H_o is the location of the FEP and FWHM is the full width at half maximum of the FEP [15:115]. The resolution of the detector at 122 keV and 511 keV for each channel are located in Table 9.

Table 9. Resolution of the NaI(Tl) detector crystals, for each channel, at 122 keV and 511 keV

	122 keV (%)	511 keV (%)
Mod 1 ch 1	19.2	6.9
Mod 1 ch 2	12.9	8.8
Mod 2 ch 0	16.9	7.2
Mod 2 ch 1	17.9	5.7
Mod 2 ch 2	16.0	7.7
Mod 2 ch 3	15.8	5.4

These resolution values are important factors in how the code used to analyze the Igor Pro output was developed.

A new $3\gamma/2\gamma$ code was developed, using MATLAB™, to analyze the data because the previous experimental setup where four detector segments gathered three photon events and two segments gathered two photon events was inefficient. The full code can be found in Appendix B. The new PsARS code was developed by combining the best features of the non-coincidence and coincidence methods. The code applied both geometry and energy filters to the data, and all six segments of the detector were used to gather two and three photon data. This reduced the runtime of the experiments and increased the detectors efficiency. In the previous setup, PMT 1 and 4 only triggered off of 2γ annihilation events and the rest of the PMT's only triggered off of 3γ events. Although plenty of 2γ photons were collected, the system was inefficient at collecting 3γ photons and thus the measurement time was long. With the new setup, all six PMT's collected general spectra, and in post processing the number of 2γ and 3γ counts is determined.

The new $3\gamma/2\gamma$ analysis code developed in this research was based on two filters, geometry and energy filters. There is no need for a time filter in the code because the settings in the code forced the modules to synchronize events and take measurements at the same time. The code starts by loading the data file and initializing the variables that record the number of 2γ and 3γ counts. There is only one 2γ geometry filter, which counts the number of events where two opposing PMT's triggered, but there are three different types of 3γ geometry filters. The first, referenced as the 120 filter, keeps track of 3γ counts that register events on every other PMT, as shown in Figure 18. The second filter, referenced as the adjacent filter, counts events where two opposing PMT's triggered and one adjacent PMT that triggered, too; an example of one such case is shown

in Figure 19. The third filter is referenced as the two count 3γ filter. It looks for 3γ photons that triggered non-adjacent PMT's. Figure 20 shows one example of the configuration. The case of only two adjacent PMT's triggering is not accounted for in the code because this case is most likely due to Compton scattering.

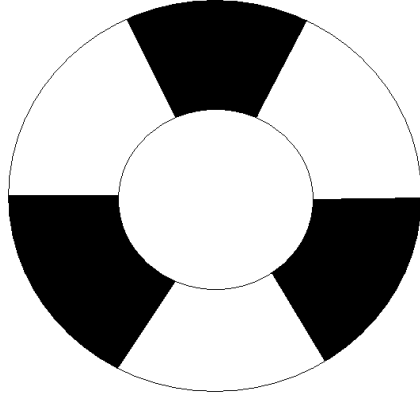


Figure 18. Diagram of the 120 degree 3γ count filter. This variable records the number of counts that occur on every other PMT. The black areas represent an area that detected an event.

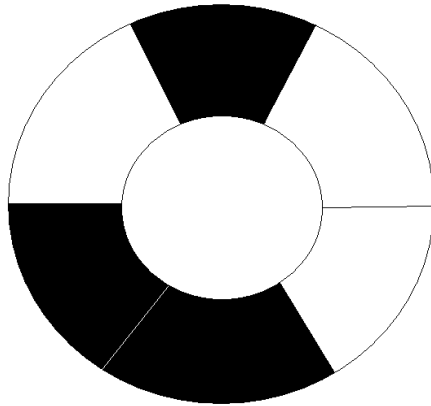


Figure 19. Diagram of the adjacent 3γ count filter. This variable records the number of counts that occur on every other PMT. The black areas represent an area that detected an event.

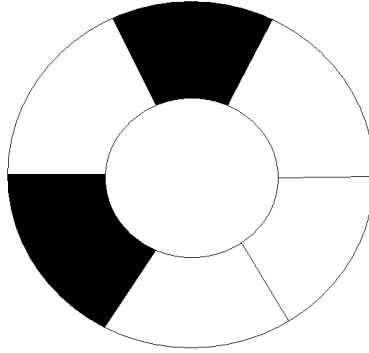


Figure 20. Diagram of the two hit 3γ count filter. This variable records the number of counts that occur on non-adjacent PMT's. The black areas represent an area that detected an event.

The next part of the code searches for the module with the smaller number of recorded events. Although the Igor Pro program synchronized the modules at the start of the experiment, malfunctions with the programs software occasionally cause one module not to record an event that the other module records. This causes the two XIA modules to have differing numbers of events. To prevent the code from crashing due to it looking for a non-existent event, the smaller module event total is chosen to run the code. Even though the events from one module to the other may not match up, coincidence events can be matched based on the XIA trigger times. Following the search for the module with the smaller number of events, the energy calibrations are added in.

Subsequently, the filter code compares the trigger times and event number to determine if the events are coincident. The code first compares the trigger times for a particular event to see if the times match. If the times do not match, the filter code uses the event in module one as the reference event and searches for the event in the second module with the matching trigger time. Next, a second time check is conducted to ensure all six times match. This second check is necessary because occasionally, a few of the trigger times within an event will be different from the others. If this happens, or no

matching time can be found, the code moves on to the next event. An example of this is shown in Figure 21.

6	0	0	42291
6	1	0	42291
6	2	0	42291
6	3	0	42291
7	0	0	65115
7	1	0	65115
7	2	0	65115
7	3	0	1512
8	0	0	2861
8	1	0	2861
8	2	0	2861
8	3	0	2861
9	0	0	21095
9	1	0	21095
9	2	0	21095
9	3	0	21095
10	0	0	32875
10	1	0	32875
10	2	0	32875
10	3	0	32875
11	0	0	38798
11	1	0	38798
11	2	0	38798
11	3	0	38798

Figure 21. An example of where times within an event will not match up for the PsARS system. The trigger time error occurs in event 7. Channels 0, 1, and 2 all have the same trigger time, while channel 3 has a different time.

The rest of the code looks for 2γ and 3γ coincidence events. For each event that has had its trigger times matched between modules, the code counts how many channels triggered. Events with only two or three total hits were analyzed. If two hits were counted, the event is first tested by the 2γ filter. The first filter is a simultaneous geometry and energy filter. It checks to see that the triggered PMT's were opposing, and that each photon was greater than 400 keV and less than 600 keV. The energy level around 511 keV was expanded to account for the energy resolution of the NaI(Tl) detector and the energy calibration. The second filter checked to make sure the sum of the energies was greater than one FEP and one Compton scatter, but less than two FEP's, 1022 keV. The Compton scatter energy was set to 150 keV. Adding this to the 511 keV

FEP, the lower energy filter level was 661 keV. However, due to the resolution of the NaI(Tl) detector at 150 keV (20%) and the lower limit of the of the 511 keV photon (400 keV), the lower energy level of 2γ filter was set to 580 keV. The upper level was set to 1124 keV based on the 10% resolution at 511 keV. If these energy and geometry conditions were met, the event was counted as a 2γ event.

If the two hit event did not pass the 2γ filter, it was then tested by the two count 3γ filter. The two count 3γ filter first applied a different simultaneous energy and geometry filter. The filter checked to see if the energies of the two non-adjacent hits were greater than the background radiation, 50 keV, and less than most probably 3γ energy, 380 keV. Like before, the 380 keV energy level was raised to 425 keV to account for the detector resolution. The code then summed up the energies of the photons and tested to see whether the total was greater than the sum of a 3γ Compton scatter and one low energy 3γ photon (200 keV), but less than two FEP's (760 keV). The lower and upper energy levels were expanded to allow for the detector resolution and set to 160 keV and 850 keV, respectively. If these two conditions were met, the event was counted as a two hit 3γ event.

The other two 3γ filters operate in the same way as the previous two. They apply a simultaneous energy and geometry filter, followed by a second total energy filter. The first 120 degree filter checks that the hits on every other detector are greater than the background, 50 keV, and less than the energy of the 120 degree 3γ photon, 340 keV. The second energy filter, within the 120 degree filter, then checks to see if the sum of the energies is greater than the sum of two FEP's energy plus one low energy 3γ photon (730 keV), but less than the sum of three FEP's energy (1022 keV). With the detector

resolution taken into account, the energy lower energy level decreased to 640 keV and the upper energy level increased to 1124 keV. The second 3γ filter is called the adjacent filter. The first adjacent filter tests has the same 50 keV and 380 keV energy levels criteria as the two count 3γ filter, except it checks that two opposing PMT's and one of the four adjacent PMT's triggered. The second filter within the adjacent filter checks to see if the sum of the energies is greater than the sum of two Compton scatters and one low energy 3γ photon (350 keV), but less than three FEP's (1022 keV). Again, each energy level was adjusted to account for detector resolution. The resultant energies for the lower and upper sum energy filter were, respectively, 308 keV and 1124 keV. Lastly, the code sums up the total 3γ counts, and outputs the number of 2γ and 3γ counts.

To correct for background radiation and accidental coincidence, an equation was developed that related the input count rate and measurement time. A Sr-85 source was measured and analyzed to develop the equation. The Sr-58 source was chosen because its gamma-ray energy is close to that of the 511 annihilation photon. Furthermore, the 514 keV gamma-rays will not undergo Doppler broadening. The 511 keV photon from Na-22 experiences Doppler broadening when the annihilating positron and electron have a momentum component along the direction the photon was measured [22]. The accidental coincidence counts arise from background radiation and cosmic rays triggering the PMT's within the coincidence window. In addition, accidental coincidence counts arise from when a 2γ or 3γ photon is coincident with background radiation or cosmic rays. When measuring the Sr-85, no true coincidence events should be happen, but accidental coincidence events will occur due to the aforementioned reasons. Therefore, a

correction for accidental coincidence can be developed that will be subtracted from the raw 3γ and 2γ counts to get the true number of counts.

The correction was produced by measuring the Sr-85 for one hour. The data was analyzed using the PsARS code to give the total number of 3γ and 2γ counts. The formula relating the measurement time and input count rate to number of accidental coincidence events takes on the form:

$$counts = xtc \quad (21)$$

where t is the measurement time, c is the input count rate, and x is a constant based on the number of accidental counts recorded from measuring the Sr-85 [20]. The reason the input count rate was chosen over the activity of the source was because the NaI(Tl) detector is very sensitive to even low activity sources and will produce pulse pile-up. For example, when the second capillary tube source was measured, the event rate was 2,964.4 counts/sec, however, the input rate into the NaI(Tl) detector was 964.5 counts/sec. Consequently the input count rate was the true measurement of the input into the detector.

3.2 Lifetime Measurements

3.2.1 Igor Pro PALS system

The lifetime measurements were conducted using PALS to measure the lifetimes of Ps formed at the surface of the gold coated capillary tube. The method uses two BaF₂ scintillation detectors connected to a Tektronics oscilloscope to trigger coincident events that occur within 100 nsec. Both of the detectors act as the start and the stop modules. As soon as one of the detectors is triggered by the 1.274 MeV gamma-rays, the PALS

program tracks the amount of time that passes until the other detector registers one of the 511 keV annihilation photons. If no 511 keV photon is detected within 100 ns, the modules reset and wait for another 1.274 MeV gamma-ray event.

The PALS software programs were developed at Eglin Air Force Base, by Dr. Michael Lindsay. The program consists of four parts, the Digital PALS program file, the PALS tool file, the VISA file, and the PALSfit program. The Digital PALS program file is responsible for gathering the lifetime data. At the beginning of the code, there is a section that lists all of the user defined detector dependent parameters. The AFIT BaF₂ parameters, as shown in Table 10, were taken from the previous version of the code, DigitalPALS_1.14.ipf, and added to the new code sent in by Dr. Lindsay, DigitalPALS_1.16.ipf. The VISA file was written to allow programs to control virtual instrument software architecture, VISA, compliant instruments connected to a computer [13]. For this experiment, the VISA file allows the Igor Pro PALS program to control and communicate with the Tektronix TDS5104B digital phosphor oscilloscope function. The tool file contains all of the non-VISA related functions need for importing, exporting, and analyzing the raw PALS data. In addition to a new version of the digital PALS codes, the PALS tools code, DigitalPALSTools_1.6.ipf, was updated. The output of the tool file is a lifetime spectrum of the PALS data. Lastly, the spectrum is analyzed using PALSfit.

Table 10. Igor Pro PALS parameters for the BaF₂ detectors

Ref voltage (V)	-1.5
Cutoff Voltage (V)	0.4
Trigger amp	0.08
DP_G width	2.6×10^{-9}
DP_G width range	0.6×10^{-9}
DP_B baseline	-0.0025
DP_V scale	0.1
DP_V position	3.8
DP_T fit before	5.0×10^{-8}
DP_T fit after	1.0×10^{-9}
Points per frame	500
Num frames	4395
DP_Ticker	58.823
DP_Pur1	0.0021
DP_Pur2	-0.0381
DP_Pur3	8.7×10^{-3}

PALSfit is a program that uses a least squares best fit routine to find the Ps lifetimes. PALSfit operates in two different modes to extract different data from the spectra [30]. The first, called PositronFit, extracts the lifetimes and intensities from the spectra. The second, called ResolutionFit, calculates the time resolution function from the spectra [30]. Both modes fit a sum of decay exponentials, convoluted with a resolution function, plus a constant background, to the spectra. Along with the spectra to be analyzed, PALSfit needs a set of input parameters to run. These parameter are best guesses of the parameters to be fitted, and may also be constraints to the parameters [30]. Once ran, the program outputs the final estimate for all the fitting parameters and their standard deviations. In addition, the program outputs three numbers that describe how well the parameters model the spectra: variance of the fit, chi-square, and significance of the imperfect model. The program can also plot the data and results together [30].

The first step in calibrating the two BaF₂ detectors involved determining the optimal operating voltage for each PMT. The electronics used were an ORTEC model 142 pre-amplifier, ORTEC model 556 high voltage (HV) power supply, ORTEC model 671 linear amplifier, ORTEC model 551 single channel analyzer (SCA), and an ORTEC model 996 counter. The electronics were connected in the same way as for the calibration of the NaI(Tl) detector, reference Figure 10. As before, a Sr-85 source was measured. To guarantee the SCA triggered on the 514 keV gamma ray, a Tektronix TDS5104B digital phosphor oscilloscope was employed to set the correct cut-off voltage. The initial voltages on the PMT's were set to -2200 V, and the counter recorded the number of counts for 10 sec. The voltage was then incremented until the number of counts peaked. The operating biases for the two detectors are located in Table 11.

Table 11. Operating biases of the two BaF₂ detectors

Serial number	Bias (V)
BA0935	-2380
BA0929	-2460

After running calibrations, a setting on the oscilloscope was changed, leading the Igor Pro program to freeze as soon as the Digital PALS code was executed. After months of unsuccessful troubleshooting, a new system was developed with the help of 1st Lt William Harrell.

3.2.2 MATLAB™ PALS system

The PALS system developed by Lt Harrell was originally designed to detect pair production and Compton scattered events from high energy gamma rays. To be able to

determine if two events are coincident, Lt Harrell developed a program, in MATLAB™, to determine the time between two incoming signals triggered in an oscilloscope. The setup involved the two BaF₂ detectors facing each other, with the radioactive source located underneath the detectors, reference Figure 22. Unlike most PALs measurements where the two detectors are each placed on one side of the radioactive source, the BaF₂ detectors are placed underneath the source because they are more efficient in this configuration. The signals from the two BaF₂ detectors then lead into two channels on a Tektronix DPO7104 digital phosphor oscilloscope, serial number B022288. Through a TekVISA application, a VISA application that allows the computer to communicate with the oscilloscope, the MATLAB™ program is able to communicate and control the oscilloscope. The instrument driver for the oscilloscope was obtained from Captain Jesse Forster, who modified a driver that controls a different model of oscilloscope because no drivers exist for the DPO7104 model. A diagram of how the electronics are connected is shown in Figure 23.

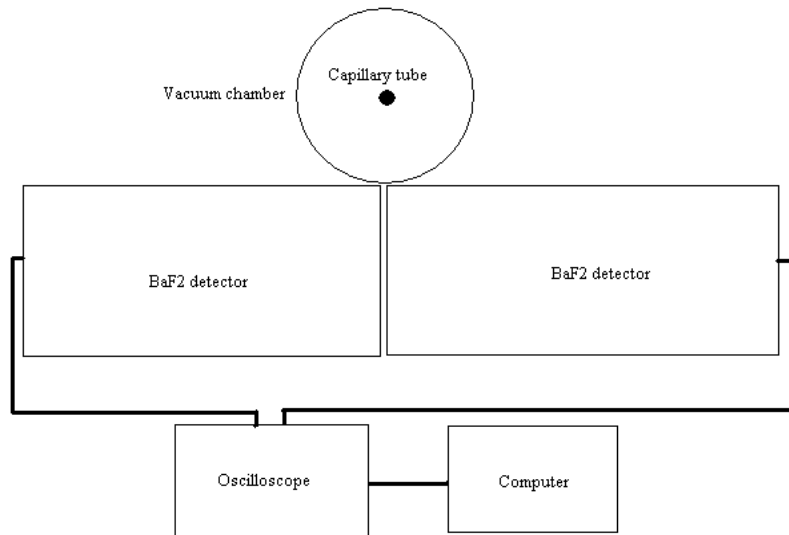


Figure 22. Setup of the PALS BaF₂ detectors with respect to the capillary tube.

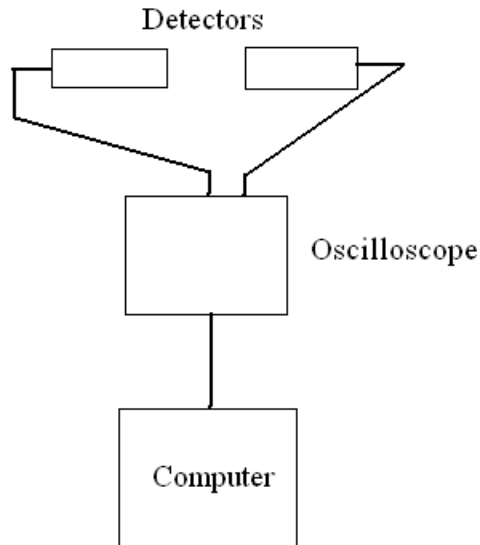


Figure 23. Diagram of how the electronics are connected together to conduct the MATLAB™ PALS experiment.

The first step in creating the lifetime code involved taking the original code developed by Lt Harrell and altering it to measure radioactive sources and produce spectra in order to calibrate the system. The initial block of code sets up communication with the oscilloscope, and initializes all of the oscilloscope parameters. Many of these parameters were set to match those in the DigitalPALS_1.16.ipf PALS code. However, some values could not be met and they were set to be as close as possible to the Igor Pro PALS values. The oscilloscope parameters are listed in Table 12. The time per division, time per point, and record length must be set on the oscilloscope by hand before running the MATLAB™ program because the program cannot set all the needed parameters.

Table 12. MATLAB™ PALS parameters for the BaF₂ detectors

mV/division	50
ns/division	20
psec/point	100
Record length	2000
Run type	High resolution
Horizontal position	20
Enhanced triggering	off
Ch 3 trigger level	-0.01
Ch 4 trigger level	-0.01

Once the connection with the oscilloscope is established, the MATLAB™ code starts collecting data, to calibrate the system, through the use of the `data_cal_stream.m` file, attached in Appendix C. The calibration code collects data through the use of an “AND” logic gate. The threshold trigger level for both channels is set to -0.01 V and the condition for the logic gate to trigger on was set to false. This makes the oscilloscope trigger on any pulse with a magnitude above 10 mV. Next, the code captures the pulse’s waveform, and saves the waveform to a file. Each time a new pulse is detected, the new waveforms are appended to the previous data file. This data file is then analyzed using the `cal_scan.m` file, located in Appendix D. This code loads the file, and then loads segments of data to be analyzed instead of loading the entire data set and then analyzing the data. This greatly reduces the runtime of the code. The faster analysis time is accomplished using the `textscan` function in MATLAB™. The `textscan` function loads the data into the `cal_func.m` function file, located in Appendix E, file and analyzes the segmented data. The `cal_func.m` file outputs the results back into the `cal_scan.m` file and the `textscan` function passes the next group of data to the `cal_func.m` file.

The `cal_func.m` function file smoothes out the waveforms using a Savitzky-Golay routine to fit the data to a ninth order polynomial using thirty-three waveform points. This setup was chosen to smooth out the noise in the data, but not so much that data is lost from the smoothing. Figure 24 shows an example of an unsmoothed waveform, and Figure 25 shows the same waveform, but smoothed. After smoothing, the code finds the location and pulse height of the waveform. Lastly, the function writes the pulse heights back to the `cal_scan.m` file. The scan file then continues to load segment data into the function file until all the waveforms have been analyzed. Finally, the code assembles and displays pulse height energy spectrum for each channel.

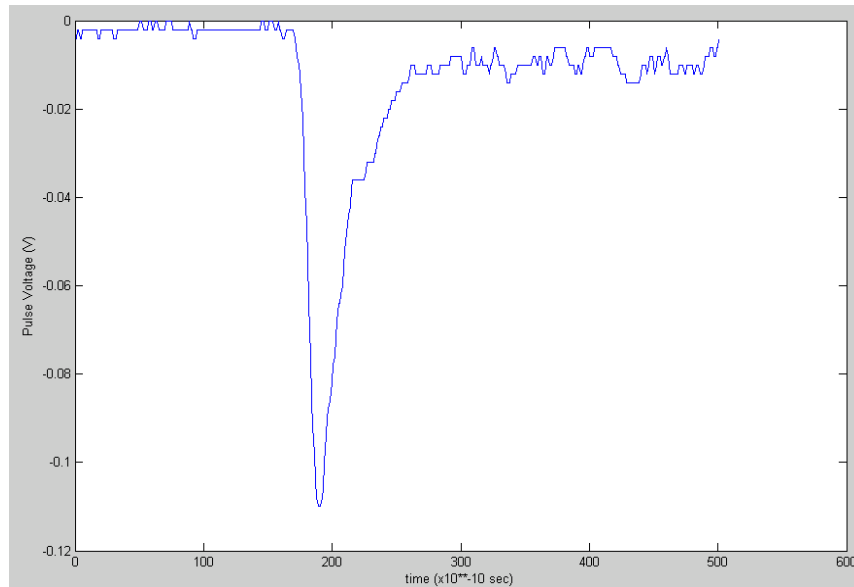


Figure 24. Unsmoothed waveform pulse from measuring a Na-22 source.

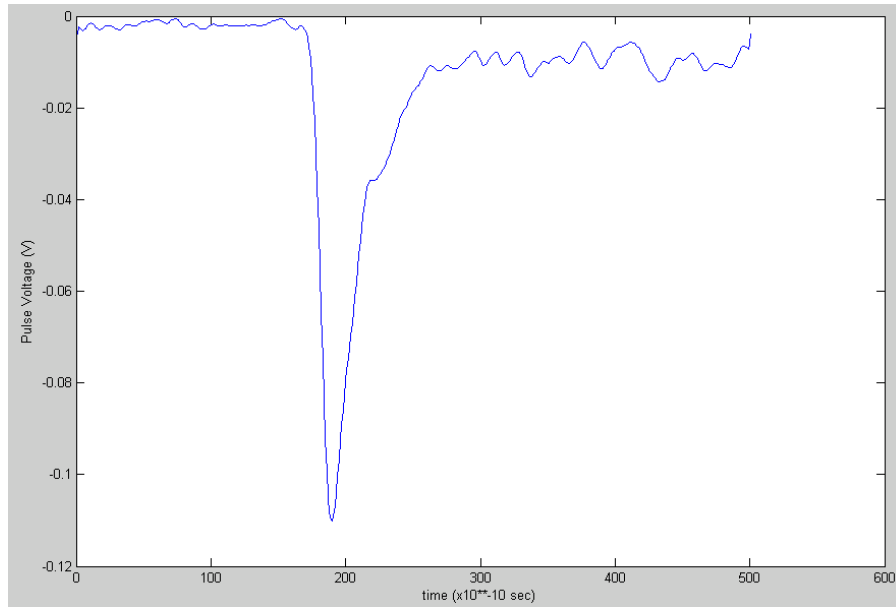


Figure 25. Smoothed waveform pulse, from measuring a Na-22 source, using a Savitzky-Golay filter. The filter smoothed the data using a ninth order polynomial using thirty-three waveform points.

From the pulse height spectra, calibration equations can be made for the detectors. To create the calibration equations for the PALS code, three sources ,Cs-137 (AFIT source number T-89), Co-57 (AFIT source number T-85), and Sr-85 (AFIT source number T-133), were measured for three hours each. All three sources are gamma ray sources and release, respectively, 662 keV, 122 keV, and 514 keV gamma rays. Figure 26 shows the Cs-137 energy spectrum.

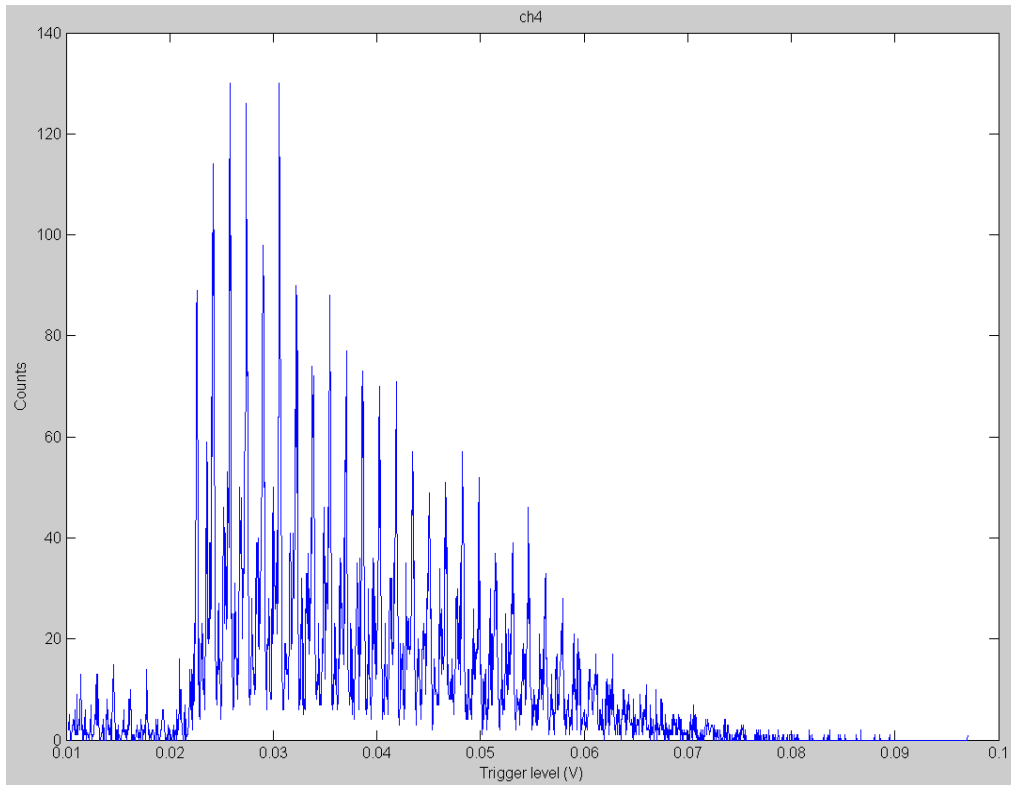


Figure 26. Energy spectrum from measuring a Cs-137 source for three hours. The 662 keV peak is located at 0.0482 V.

From looking at the Cs-137 spectrum, it is evident that there is a bias in the system that causes certain trigger level bins to collect more counts than others. The bias is caused from the rounding off of the pulse voltage in the oscilloscope. Furthermore, this problem is aggravated by the system not having enough resolution when the data is digitized. Due to the poor energy spectra and the large error associated with identifying the FEP for each isotope, the calculated energy calibration equations did not correctly identify the trigger voltages for the 511 keV and 1274 keV photons. Instead of creating a calibration equation to convert the trigger levels into energies, the PALS code ran directly off of the trigger level voltages. The correct trigger levels were determined by examining a Na-22 source on the oscilloscope in infinite persistence mode to identify the voltages. The 511

keV photon was set to trigger on -35 mV and the 1274 keV photon on -95 mV, but were raised, respectively, to -10 mV and -60 mV to account for the poor energy resolution of the BaF₂ detectors.

With the calibrations complete, Lt Harrell's original code was modified again to create the new PALS code. As before, the first code sets the parameters on the oscilloscope and streams in the data. This code is called `Stream_data_PALS.m`, and is located in Appendix F. However, this code does not use the "AND" logic gate like before. This code uses a setup and hold trigger mode. With this setup, the first channel acts as the start module and triggers off of pulses greater in magnitude than 60 mV. The first trigger acts as the clock source and once it triggers, off of the 1274 keV photon, the clock stays open either for 100 ns, or until the second channel triggers. Off of the 511 keV photon. The second channel acts as the stop module and triggers off of pulses greater in magnitude than 10 mV. During the time the clock remains open the oscilloscope records the waveforms for both pulses. If a second pulse was detected within 100 ns that met the energy criteria, the two waveforms were sent to the stream file to be saved. If a second pulse was not detected, the oscilloscope reset and waited for another start signal to begin recording data again.

Once the data is collected, the data file is analyzed using the `PALS_meas.m` file, located in Appendix G. This file opens the data file, and sends segmented data to the `PALS_func.m` file., located in Appendix H. This file smoothed and applied energy calibrations to the data. Next, the data was passed to a second function file, `find_midrise_time.m`, which is located in Appendix I. The function found the location in the waveform where the pulse reaches 50% of its maximum, then reported the time for

that location. The midrise time of the pulse, rather than the time of the pulse peak, was used as the time of the pulse because the noise in the waveform changed the location of the pulse peak. Next, the code checked to see if the difference between the two midrise times were less than the 100 ns window. If they were, an energy filter was applied to check to ensure the first pulse was the 1,274 keV start pulse and the second pulse was the 511 keV stop pulse. If the energy criterion were met, the difference between the two times was reported as the lifetime of that Ps annihilation event. Lastly, all the lifetime data was passed back to the PALS_meas.m file and the data was plotted as a lifetime spectrum. This data can then be analyzed using PALSfit as well to determine the annihilation lifetimes contributions in the PALS spectrum

3.3 The Capillary Tube

The capillary tubes were chosen for this research because of their ability to both contain the radioactive Na-22 solution and moderate the positrons. The tubes were custom-made of silica with an inner layer of silver. On top of the silica is a layer of polyimide. An outer layer of gold was added later by Lt Slaughter. Two different tubes were procured, each with a different thickness of silica. The lighter colored tube has a silica thickness of 65 μm and the darker colored tube has a silica thickness of 75 μm , reference Figure 27.

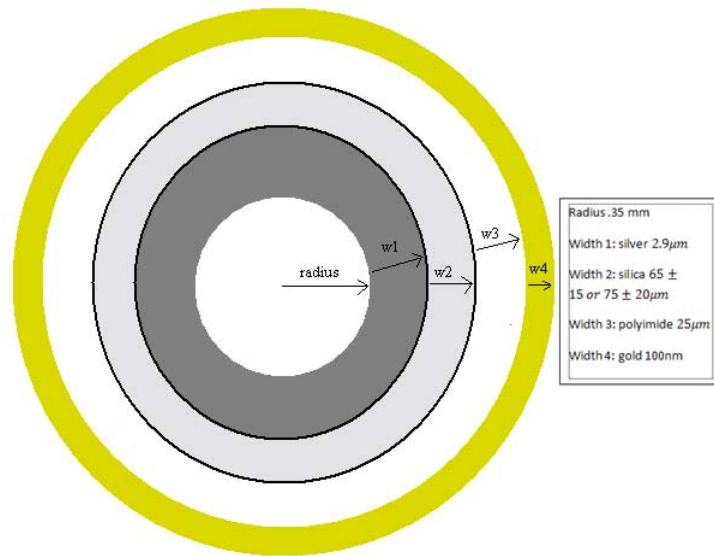


Figure 27. Cut away diagram of the custom made capillary tubes showing each material and its thickness.

In Lt Slaughter's experiments, the results were affected due to the fact that the capillary tube was not centered inside the vacuum chamber. The capillary tube was attached on one side to the vacuum chamber wall, but left unattached on the other side, allowing the unattached end of the capillary tube to bend downward under the force of gravity. Figure 28 diagrams a device to hold the free end of the capillary tube up. The ring was designed, by me, to have a hollow center to reduce the amount of mass escaping positrons could interact with. Fishing line was strung across the vertical and horizontal holes to create a square of line in the middle that will hold the free end of the capillary tube in the center of the vacuum chamber.

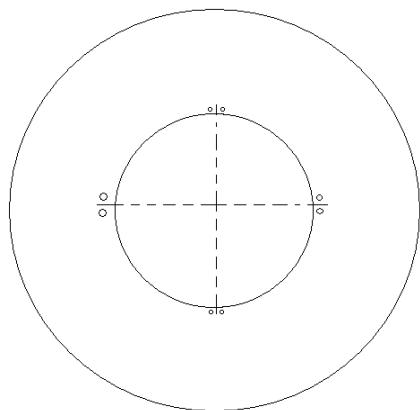


Figure 28. Diagram of polyethylene ring designed to hold the capillary tube in the center of the vacuum chamber. Across the vertical and horizontal holes is strung fishing wire to hold the capillary tube in place. The outer diameter is 1.350 inches. The inner diameter is 0.85 inches. Each small hole has a diameter of 1 mm. Each of the holes is located 3 mm from edge of the inner radius, and 1 mm off the vertical and horizontal lines coming from the center. The thickness of the ring is 0.25 inches. The ring is constructed of polyethylene.

The capillary tube is housed in a vacuum chamber system to reduce the amount of atoms and molecules escaping positrons could interact with. It is attached at one end to a high voltage feed through and the HV feed through is connected to a 10 inch ConFlat flange (CF) nipple, constructed by Kurt J. Lesker. Wires connecting the inside silver layer and outside gold layer of the capillary tube each connect to a voltage feed-through to allow external biases to be applied to the layers. After the nipple in the system is a Gamma Vacuum 10S ion pump, followed by a valve, a Drytel 1025 roughing pump, another valve, and finally a Varian multi-gauge vacuum, sensor. The roughing pump will pump the pressure in the chamber down to 10^{-3} - 10^{-4} torr. Once the pressure reaches 10^{-4} torr, the ion pump can be turned on to reach pressures of 10^{-7} torr. A tee can be exchanged for a cross in the middle of the system to allow a second experiment to be going on in the other side of the system, and the two valves on both sides of the roughing pump can isolate one side of the system. Figure 29 shows a picture of the setup.

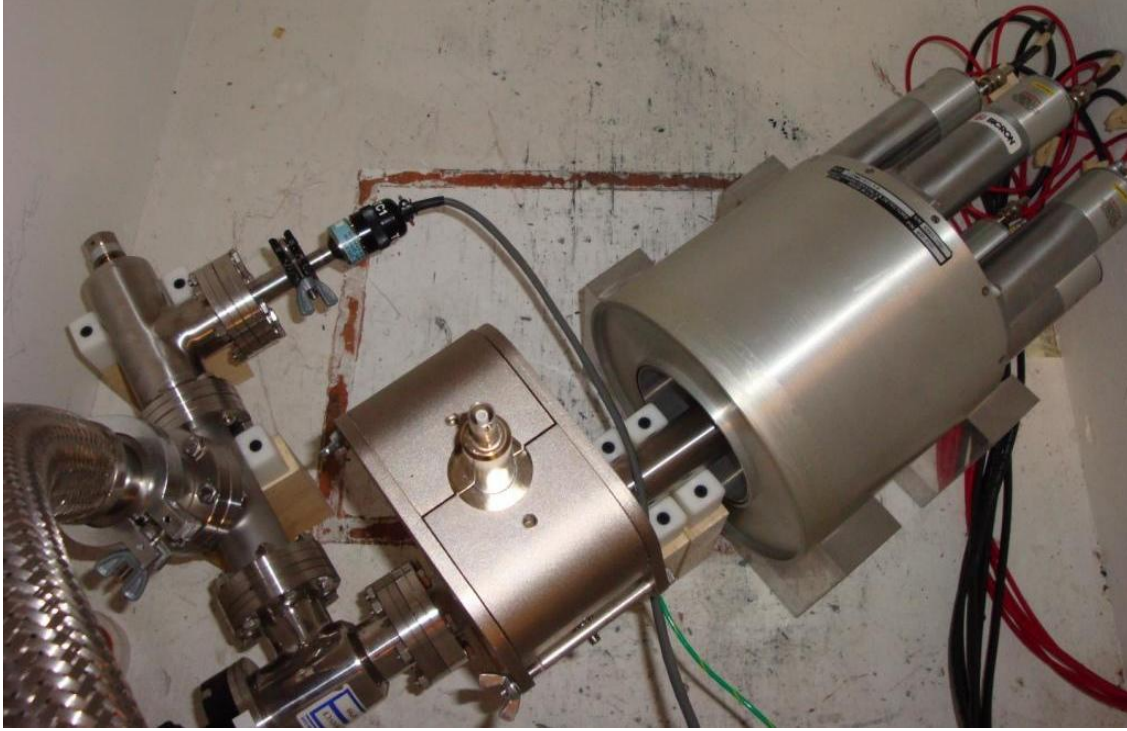


Figure 29. Experimental setup of the PsARS system with the capillary tube centered inside the NaI(Tl) detector.

From Figure 6, a majority of the o-Ps formation can be suppressed inside the polymer by applying a 50kV/cm electric field across the capillary wall. Larger fields will decrease the o-Ps further, but with diminishing returns. Above 50 kV/cm, larger and larger electric fields reduce the o-Ps formation by increasingly smaller amounts. To determine the approximate biases needed to achieve a 50 kV/cm, field, the silver and gold layers are modeled as a cylindrical cathode and anode. Because the cathode and anode are cylindrical, and not parallel plates, the electric field is not uniform. The electric field from a cylindrical capacitor calculated:

$$E(r) = \frac{V}{r * \ln\left(\frac{b}{a}\right)} \quad (22)$$

where V is the applied voltage between inner and out cylinders, a is the inner cylinder radius, b is the outer cylinder radius, and r is the location at which the electric field is calculated [15:162]. For the capillary tube, the inner radius is 3.5×10^{-4} m and the outer radius is 4.529×10^{-4} m. Because the positrons are going to be brought to the outside surface of the gold surface, r equals 4.53×10^{-4} m. By calculating the electric field at varying voltages applied to the silver layer, the voltage needed to obtain an electric field of 50 kV/cm will be known, reference Figure 30.

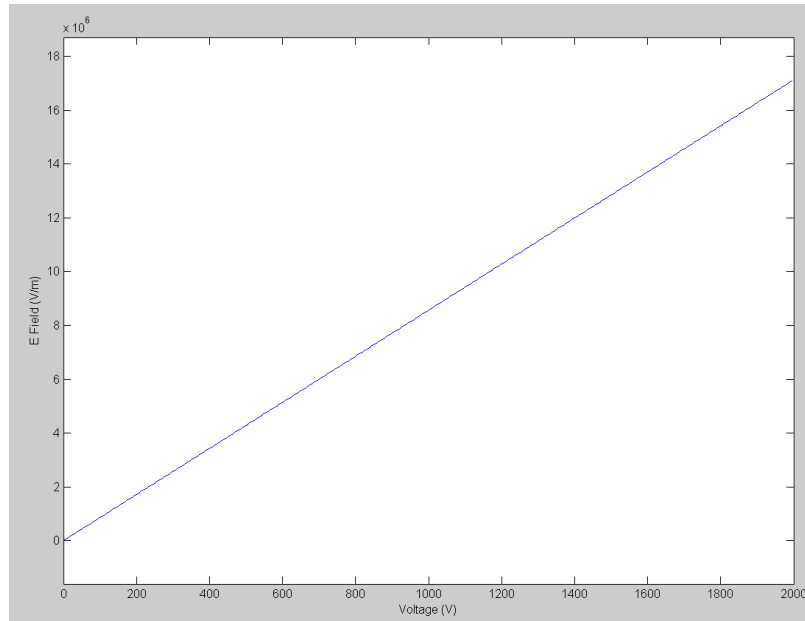


Figure 30. Calculation of the electric field at the top of the gold surface on the capillary tube with varying voltages applied to the silver layer.

From Figure 30, an electric field of 50 kV/cm will be obtained by applying a bias of approximately 600 V to the silver layer. However, this value is only an estimate of the true value because the silver and gold layers are not perfect cylinders and the gold layer is not 100 nm thick over the whole capillary tube. Furthermore, the calculation does not

account for the dielectric in-between the silver and gold layers. This calculation is only used to estimate the approximate bias needed on the silver layer.

The gold was added to the capillary tube, by Lt Slaughter, using the torr Electron Beam Evaporation System (E-Beam) [2:65]. To determine the smoothness of the gold layer on the capillary tube, the tube was scanned using an atomic force microscope, or AFM. The AFM works through the use of a cantilever with one end having a sharp tip. The tip of the cantilever was made of diamond with a diameter of 100 nm [2:73-5]. The AFM was used to scan a 2000 nm region on the capillary tube that was previous determined to be smooth with no bumps. In previous scans, different areas of the capillary tube had bumps as large as 40 nm on the surface [2:73-5]. Figure 31 shows the change in surface roughness.

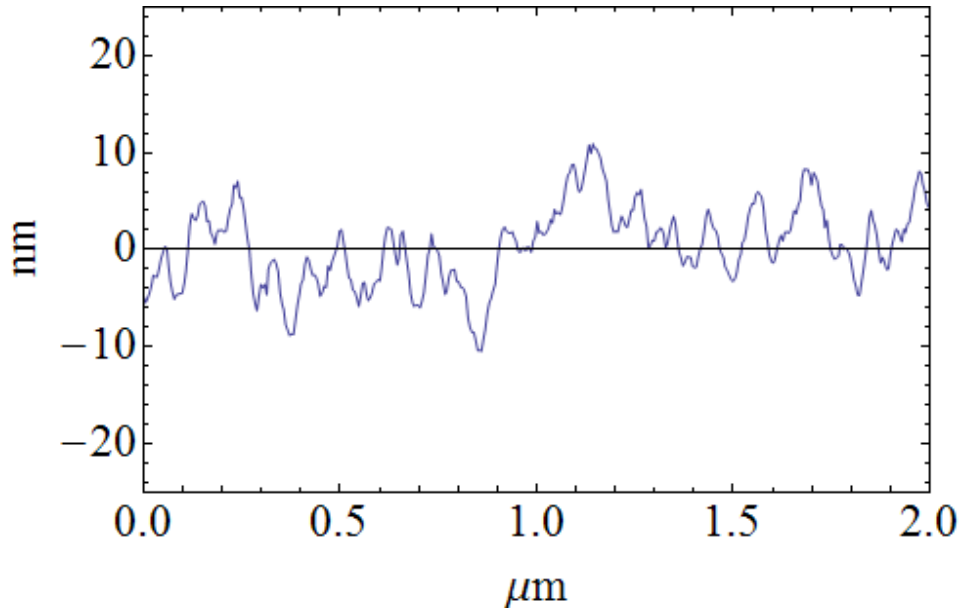


Figure 31. Plot of surface roughness over a 2000 nm smooth region of the capillary tube gathered using an AFM [2:75].

Each typical feature, or peak, size is about 100 nm in the lateral dimension and 10 nm in height. Over the 2000 nm region, the average change in surface thickness never exceeds 20 nm. Although the surface roughness makes estimating the electric field difficult, it will prove useful once the polarizing electric field is applied [2:73-75].

To polarize the Ps on the surface of the gold, an electric field of approximately 120 kV/cm will be needed [16]. To calculate the needed bias, equation 22 was used. For this case, the gold layer is the inner cylinder and the vacuum chamber wall is the outer cylinder because it is the location of the ground. R equals 4.53×10^{-4} m, “a” equals 4.53×10^{-4} m, and “b” equals 1.715×10^{-2} m. By calculating the electric field at varying biases, Figure 32 was obtained:

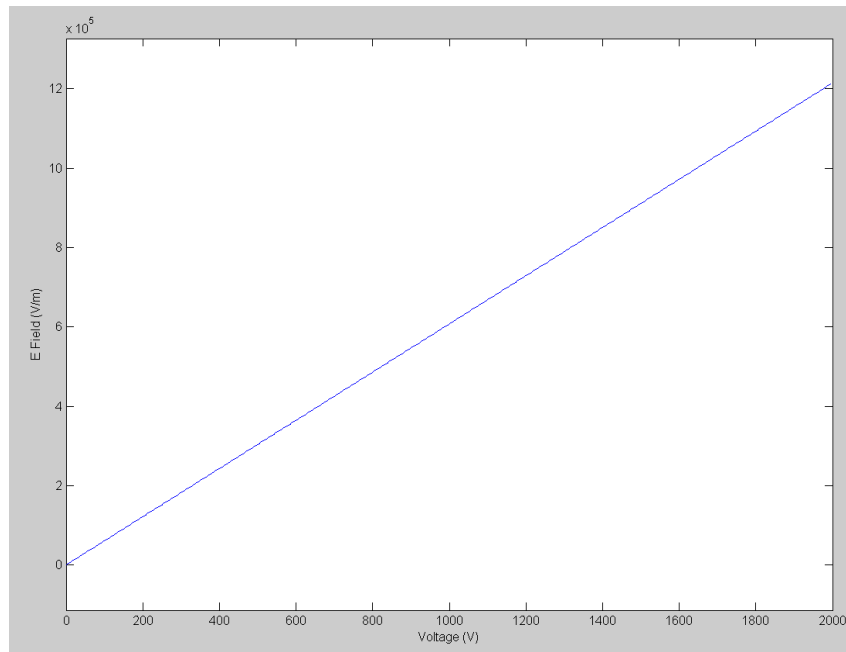


Figure 32. Calculation of the electric field at the top of the gold surface on the capillary tube with varying voltages applied to the gold layer.

As can be seen from the graph, the values of the electric field, obtained from applying the voltages, to a different location, are one to two orders of magnitude lower than the previous calculation. This is because as the location of the inner cylinder changed from the silver to the gold layer and the radius of the layer increased. The electric field is highly dependent on the radii of the cylinders and the radius of the outer layer increased by two orders of magnitude. To achieve an electric field of 120 kV/cm, a bias of approximately 20 kV is needed. This cannot be achieved with the current power supplies in the laboratory. However, because the gold coating on the capillary tube is not perfectly smooth, the differing heights of the surface may create localized electric fields on the surface that will reach the needed 120 kV/cm [29]. These high localized electric fields will be used to polarize the Ps, increasing the annihilation lifetimes. Figures 33 diagrams how the biases were applied to the inner and outer metallic layers of the capillary tube.

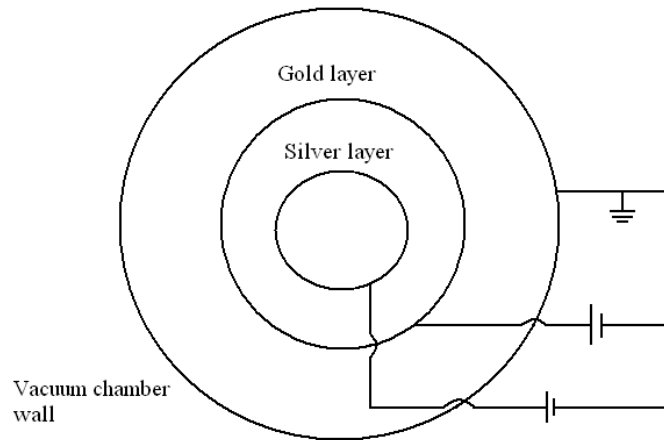


Figure 33. Diagram showing the location of where the inner and outer voltages are applied to the capillary tube.

From the previous year, to deposit the Na-22 on the inner wall of the tube, Lt Slaughter used an evaporative method. Using a 22 gauge syringe radioactive $^{22}\text{NaCl}$ was deposited inside the tube. Due to the long time that was need for the liquid to evaporate, the tube was heated using a hot plate. 0.26 μCi of Na-22 was intended to be deposited inside the tube, however, much of the NaCl escaped from the capillary. Lt Slaughter determined an activity of only 0.10 μCi remained inside the tube. Next, he used the torr Electron Beam Evaporation System (E-Beam) to deposit the gold on the surface of the capillary tube. Lastly, he attached the capillary tube to the inside of the vacuum tube [2:112]. Through the use of multiple voltage feed-through's, Lt Slaughter demonstrated that electrical contacts could be made both in the inside and outside of the capillary tube to produce a voltage difference across the wall. He used a 22 gauge electrical wire to make the first connection between the silver on the inside of the tube and one electric feed-through. The second connection was made by wrapping the gold tube and a 22 gauge wire with a thin electrical wire, and soldering the 22 gauge wire to a second voltage feed-through [2:112].

During the deposition of the Na-22 into the first capillary tube, more than half of the Na-22 escaped the tube. Lt Slaughter made the capillary tube only have contact with the hot plate on one side of the tube. This caused a pressure build-up inside the tube and ejected the Na-22 out. A second capillary tube was created this year to test a new method of Na-22 deposition. 85 μL , approximately 0.3 μCi , of the radioactive Na-22 solution was injected into a new capillary tube using a 22 gauge syringe. The tube was then placed on two stands that rested on a hot plate. Aluminum foil was placed on the hot plate to prevent the hot plate from getting contaminated. The foil was also used to create

two contacts on which the capillary tube would rest. The heat would travel from the hot plate, through the two metal contacts, and heat both ends of the capillary tube. By heating both ends of the tube instead of just one, it is theorized that the pressure will not build up inside the tube and the NaCl solution will not be expelled from the tube.

3.4 Copper Standard Source and $3\gamma/2\gamma$ Correction Factor

To correct for the different efficiencies at which the NaI(Tl) detector captures a 2γ photon versus a 3γ photon, a photoelectric absorption correction is needed. Due to its lower energy, a 3γ photon is easier to capture than a 2γ photon, but it is harder to capture all of the three 3γ photons than the two 2γ photons. To account for the difference in requiring the capture of both 2γ photons but not all three 3γ photons, a geometry correction is also needed. In addition, the 3γ photon peak lies on top of the 511 keV Compton continuum, and because they are not emitted collinear, they are harder to identify than the 2γ photons. This is corrected by adding in an energy correction factor. However, all of the correction factors can be combined into one correction factor, the $3\gamma/2\gamma$ correction factor.

The $3\gamma/2\gamma$ correction factor was calculated by measuring a standard source with a known $3\gamma/2\gamma$ ratio. Single crystal copper is a metal with a known $3\gamma/2\gamma$ ratio, 1/372. The source was created by heating a copper plate on a hot plate. Slowly, 85 μL , 0.3 μCi , of the liquid radioactive Na-22 was deposited onto the copper. The heat from the hot plate evaporated the liquid. Next, a second copper plate was placed onto of the first to sandwich the Na-22 between the copper. This was then sealed inside tape to prevent air from interacting with the copper. By collecting the spectra from the copper source and

calculating the experimental $3\gamma/2\gamma$ ratio, the known ratio is divided by the experimental ratio to determine the correction factor. Figure 34 shows what the standard source looks like. Given the accidental coincidence correction and the $3\gamma/2\gamma$ correction factor, the $3\gamma/2\gamma$ ratio can be calculated. The raw number of 3γ and 2γ counts is found from analyzing the data. After the background is subtracted, the 3γ counts are divided by the 2γ counts and multiplied by the $3\gamma/2\gamma$ correction factor to determine the actual $3\gamma/2\gamma$ ratio.



Figure 34. Picture of the copper standard source used to calculate the $3\gamma/2\gamma$ correction factor.

This section of the document described the key differences between the PsARS and PALS systems. The PsARS system used a NaI(Tl) ring detector to maximize the amount of photons collected while the PALS system used fast BaF₂ detectors to be able to resolve the time difference between the 1,274 and 511 keV photons. In addition, a standard source and accidental coincidence equations had to be created to calibrate the PsARS system. The next section will discuss the results from measuring the copper standard source, Sr-85 source, and capillary tube.

4. Results and Analysis

Once each system was setup and calibrated, initial data runs had to be completed before analysis of the capillary tube could begin. These include gathering information to compute the accidental coincidence correction counts and the $3\gamma/2\gamma$ correction factor. This information was then used to conduct the $3\gamma/2\gamma$ ratio and lifetime analysis of the capillary tube.

4.1 Accidental Coincidence Correction

The accidental coincidence equation coefficients were calculated by measuring and analyzing a Sr-85 source. The Sr-85 source was measured for one hour and analyzed using the $3\gamma/2\gamma$ code. By entering in the Sr-85 input count rate, total number of 3γ and 2γ counts, and measurement time into equation 21, the coefficients for the 3γ and 2γ equations were calculated. Given that the input count rate from the Sr-85 was 3200 counts/sec, the measurement time was 3600 sec, and the 3γ and 2γ accidental counts, respectively, equaled 5 and 35, the 3γ and 2γ accidental count equations are:

$$\begin{aligned} 3\gamma_{accid} &= 4.3403 \times 10^{-7} ct \\ 2\gamma_{accid} &= 3.0382 \times 10^{-6} ct \end{aligned} \tag{23}$$

where c in the input count rate and t is the measurement time. Three total measurement times were used: 2.0 hours, 3.0 hours, and 3 hours and 15 minutes, to measure the capillary tube. With an input count rate of 220 counts/sec, the accidental coincidence counts for the three times are listed in Table 13.

Table 13. 3γ and 2γ accidental coincidence counts for three different total measurement times of the capillary tube.

Time (hrs)	3γ counts	2γ counts
2	1	5
3	1	7
3.25	1	8

Each of the accidental coincidence counts is low due to the low activity of the capillary tube. For the 3γ counts, the 2 hour count estimate was rounded up and the 3 and 3.25 hour counts were rounded down. Differences in the 3γ counts will only be seen when measuring for longer periods of time or on higher activity sources. Due to the low activity of the source and short measurement time, the error associated with each count, especially the 3γ counts, are large. When calculating the $3\gamma/2\gamma$ ratio, each of these accidental coincidence counts will be subtracted from the raw counts to achieve the true number of counts. The low number of accidental counts is a positive confirmation that the criteria for determining if an event was a 2γ or 3γ event were successful. However, the 3γ counts have more error than the 2γ counts because of the low numbers. For two hours, the calculated accidental 3γ count was less than one, but rounded up to one. For the other two times, the 3γ counts were calculated to be greater than one, but were subsequently rounded down.

4.2 $3\gamma/2\gamma$ Correction Factor

With the ability to subtract out the background radiation, the copper standard source was measured using the NaI(Tl) detector to create the $3\gamma/2\gamma$ factor. The copper source was measured for three hours and fifteen minutes. The data was analyzed using the PsARS code to calculate the total number of 3γ and 2γ counts, respectively, to be 546

and 42395. Thirteen separate measurements were conducted to obtain these sums. The error in the counts was calculated by dividing their standard deviations by the square root of the number of measurements. Dividing the number of 3γ counts to 2γ counts yielded an experimental $3\gamma/2\gamma$ ratio of 0.012858. Dividing the actual ratio, $1/372$, by the experimental ratio yields the correction factor, 0.2090707. Equation 24 shows how the correction factor is calculated.

$$c = \frac{\left(\frac{1}{372}\right)}{\exp\frac{3}{2}} \quad (24)$$

where c is the correction factor and $\exp\frac{3}{2}$ is the experimental $3\gamma/2\gamma$ ratio. The errors in the number of counts were then used to calculate the error in the correction factor, σ_c .

$$\sigma_c = \left(\frac{1}{372}\right)(c * |p| * \frac{\sigma_{\exp\frac{3}{2}}}{\exp\frac{3}{2}}) \quad (25)$$

Where $\sigma_{\exp\frac{3}{2}}$ is the error in the experimental $3\gamma/2\gamma$ ratio and p is the power of the correction factor. Because the actual $3\gamma/2\gamma$ ratio is multiplied by the experimental ratio raised to the power of negative 1, p equals the absolute value of negative one. The error in the correction factor was calculated to be 0.00024, or 0.115% of the value of the correction factor.

In addition to the correction factor, the activity of the copper standard source was determined experimentally as well. The source was measured using a high purity germanium detector, serial number 10013369. The copper source and a standard Na-22 source were placed on top of the detector. By measuring the two sources together, the

511 keV FEP from the energy spectrum was the result of the photons from both sources. Because the activity of the Na-22 standard source is known, the source can be measured using the HPGe detector separately, and the activity of the copper source can be calculated:

$$Activity_{unknown} = \frac{Activity(^{22}Na)}{counts(^{22}Na)} * counts(Cu + ^{22}Na) \quad (26)$$

where the number of Na-22 counts will be determined from measuring the Na-22 only and the Cu plus Na-22 counts will be calculated from measuring the two sources together. After measuring the Na-22 source for five minutes, 1.46×10^6 counts were recorded under the 511 keV FEP. From measuring the two sources together, for five minutes using the same geometry, 1.48×10^6 total counts were recorded. Subtracting the Na-22 standard counts from the total counts resulted in 2.0×10^4 copper standard source counts. The activity of the Na-22 was 53.96 μCi on 1 Jan 05. After accounting for decay, its current activity is 10.824 μCi (10 Jan 11). Plugging these values into equation 26, the activity of the copper standard source is approximately 0.15 μCi (10 Jan 11). The desired 0.3 μCi was not deposited due to the error associated with extracting the Na-22 solution using a syringe.

4.3 $3\gamma/2\gamma$ Ratio Results

The first $3\gamma/2\gamma$ ratio measurements were conducted by applying a voltage bias on the inner silver layer with the ground set to the vacuum chamber wall. All of the measurements were conducted under a vacuum pressure of 1.36×10^{-3} torr. The bias was chosen to be positive on the inner silver layer because the positrons are positively charged. Using a positive bias, the electric field will push positrons in the direction from

the silver layer to the gold layer. This tends to force the positrons to travel from the inner portions of the capillary tube towards the gold layer. An initial ratio baseline was conducted by applying no voltage, and then data was collected with the voltage incremented up to 1 kV, in steps of 200 V. However, data was collected at addition biases to fill in the gaps of the data. Each data point was initially measured eight times for fifteen minutes, or for a total of two hours. However, to decrease the error in the measurements at the lower voltages to better see what was happening, an additional four measurements were conducted. These short measurement times were chosen to minimize the output data file sizes. For larger run times, the output files were too large to open and the file information located at the top and middle of the files could not be deleted. The following results were obtained:

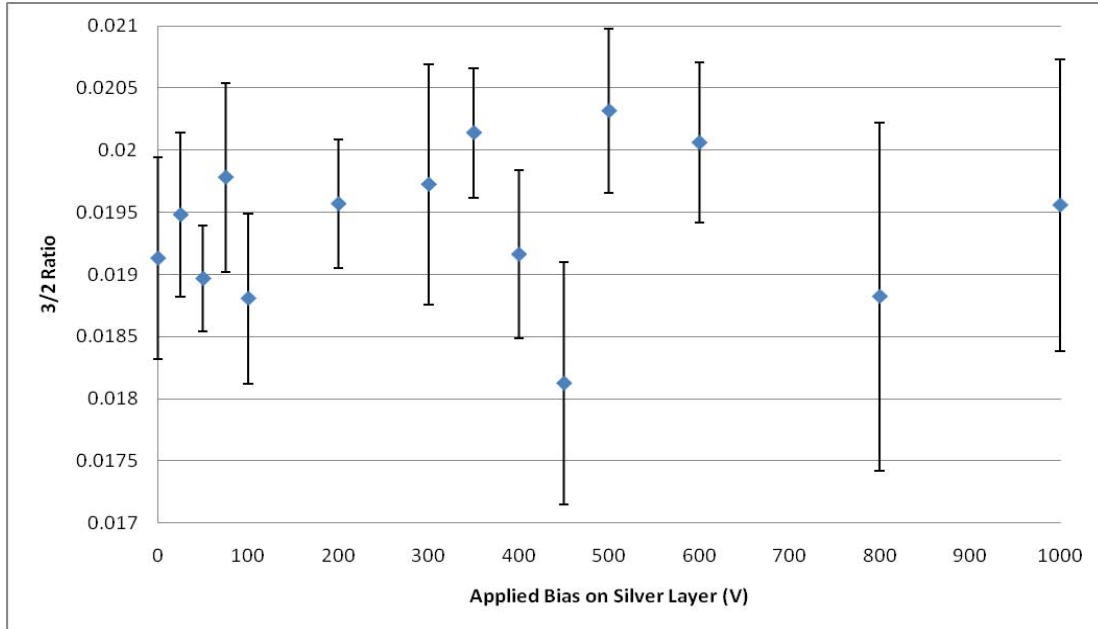


Figure 35. $3\gamma/2\gamma$ ratio results by applying a voltage bias on the inner silver layer of the capillary tube. The ground was established at the vacuum chamber wall.

The results show that the $3\gamma/2\gamma$ ratio remains fairly constant up to 300 V, then rises at 350 V, decreases at 450 V, and then above 450 V increases again. The change in the $3\gamma/2\gamma$ ratio between 300 and 450 V show that applied voltages are influencing the $3\gamma/2\gamma$ ratio, but the constant ratio before 300 V show that the ratio is changing, but something is interfering with the measurements. However, as the bias continued to increase above 450 V, the results show that the bias was strong enough to eject the positrons out of the capillary tube. At high voltages, the electric field was able to impart enough energy to the positrons so that they could overcome the potential barrier and the gold surface, and escape. Once escaped, they either annihilated with molecules or atoms in the air, or at the vacuum chamber wall. The rise in the $3\gamma/2\gamma$ ratio was because the gamma rays were being measured off center. When the 2γ photons were produced at the center of the detector, they were released 180 degrees apart and detected by opposing PMT's. However, when the positron annihilated off center, the 2γ photons were not detected by opposing PMT's; they were mistaken for 3γ counts and falsely increased the $3\gamma/2\gamma$ ratio.

The interference problem at lower voltages arose due to the fact that the ground was applied to the vacuum chamber wall and not the outer gold layer. With a bias applied to the silver layer, and the gold layer left ungrounded, the gold layer acted as a shield and prevented the voltage from dropping across the capillary tube. Instead of the voltage drop across the capillary tube, the bias on the silver layer charged the gold layer, and the majority of the voltage drop occurred from the gold layer to the vacuum chamber wall. A small experiment was conducted to test this theory. The inner applied voltage on the silver layer was set to 50 V and the gold layer was left ungrounded. The voltage drop

across the two layers was .001 V, but the voltage drop from the silver layer to the vacuum chamber wall was 50 V. When the gold layer was established as ground, the voltage drop across the silver and gold layer increased to 45 V, proving that with the ground established at the gold layer, the voltage drop across the capillary tube is known. The 45 V drop across the silver and gold layer is a best estimate because the multi-meter used to measured the voltage does not have an impedance high enough to limit the current it draws from the circuit, thus lowering the readout. To better see what was happening with the $3\gamma/2\gamma$ ratio at low applied voltages, a second experiment on the capillary tube was conducted with the ground established at the gold layer.

By establishing the ground at the gold layer, the voltage drop across the capillary tube was known and the low voltage $3\gamma/2\gamma$ measurements were repeated. Like the previous experiment, the measurements were conducted under vacuum, with a pressure of 1.36×10^{-3} torr. Each data point was obtained by measuring the capillary tube for a total of three hours made from twelve separate measurements. The new $3\gamma/2\gamma$ ratios are:

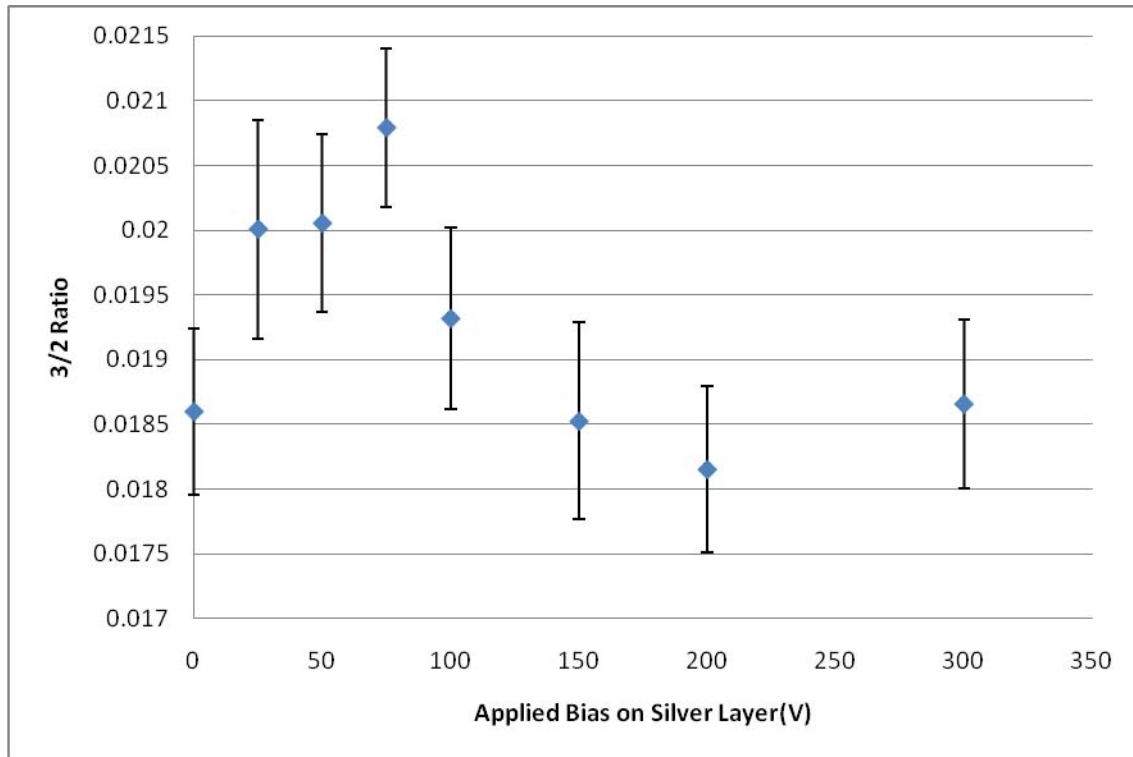


Figure 36. $3\gamma/2\gamma$ ratio results by applying a voltage bias on the inner silver layer of the capillary tube. The ground was established at the outer gold layer.

The results clearly show that the $3\gamma/2\gamma$ ratio rises, then falls. The peak $3\gamma/2\gamma$ ratio occurs at 75 V. This peak is the voltage that gives the positrons enough energy to lie at the top of the Ore gap as they traverse through the capillary tube. Beyond this voltage, too much energy is given the positron and as it ionizes an atom during its travel, the positron imparts too much energy to the electron and the electron escapes before the positron can capture it and form Ps. To determine whether the change in the $3\gamma/2\gamma$ ratio is influenced more by the number of 3γ or 2γ counts, the number of counts are graphed in Figures 37 and 38. The error data points were calculated by taking the square-root of the number of counts.

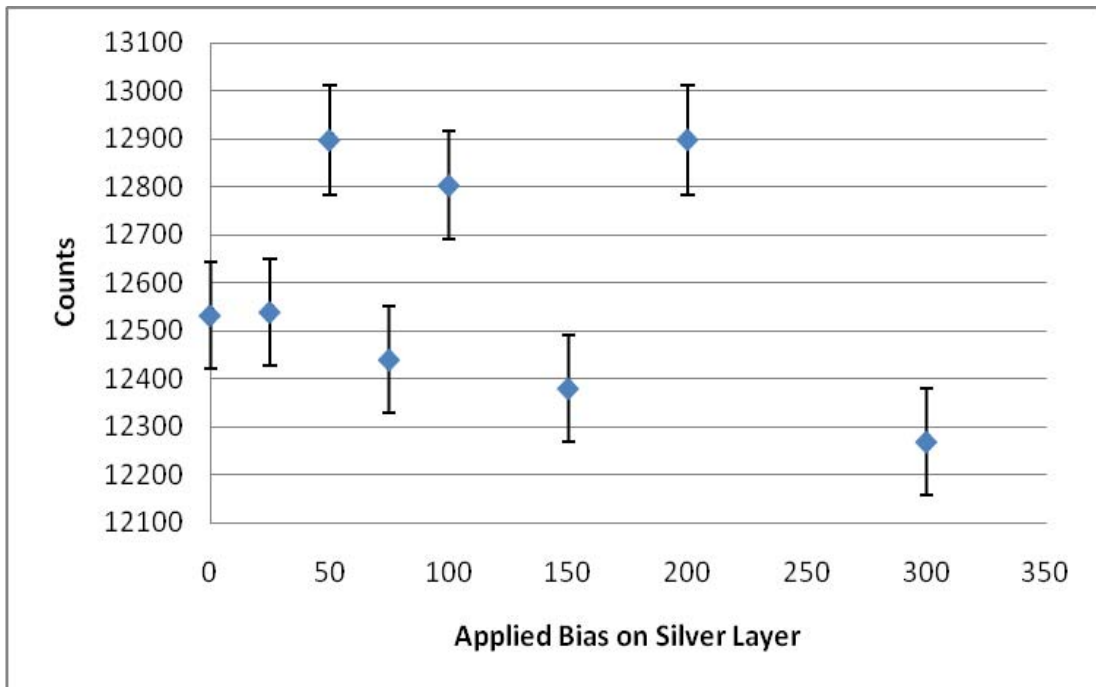


Figure 37. Number of 2γ counts from the $3\gamma/2\gamma$ ratio experiment with the ground applied to the gold layer.

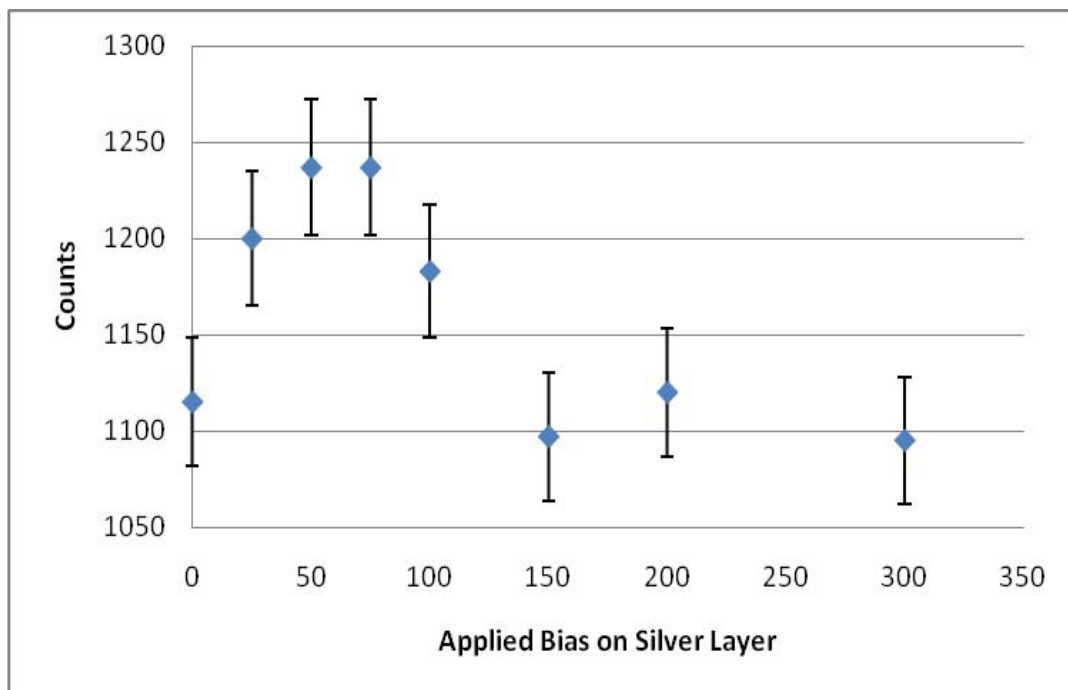


Figure 38. Number of 3γ counts from the $3\gamma/2\gamma$ ratio experiment with the ground applied to the gold layer.

In Figure 37, there is no distinct pattern in the data, the data is approximately constant when the error bars are expanded from 1 sigma to 3 sigma. As the $3\gamma/2\gamma$ ratio peaks, then decreases, the number of 2γ counts does not peak and then decrease. In Figure 38, the data for the 3γ counts follow the same rise and fall pattern of the $3\gamma/2\gamma$ ratio data. This implies that the number of 3γ counts influences the $3\gamma/2\gamma$ ratio, and not the number of 2γ counts. The decrease in o-Ps counts is the result of either the electric field causing the o-Ps to not form, or the electric field is increasing the rate of o-Ps pick off annihilation. However, this determination cannot be made until lifetime analysis is conducted on the data.

The voltage drop of 75 V was used in the subsequent outer applied bias experiment. In the second experiment, two biases were used, one on the silver and one on the gold layer. The first bias on the silver layer will still push the positions to the surface of the capillary tube, and the second bias will create an electric field that will polarize the Ps on the gold surface. However, instead of applying a 75 V bias to the silver layer, the inner and outer biases were adjusted to achieve a drop of 75 V from the silver to the gold layer. The grounds for each bias were established at the vacuum chamber wall. As before, the thirteen measurements, fifteen minutes each, were conducted to gather each data point and the measurements were conducted under a vacuum of 1.36×10^{-3} torr. The $3\gamma/2\gamma$ ratios with an inner and outer field applied to the capillary tube are shown in Figure 39.

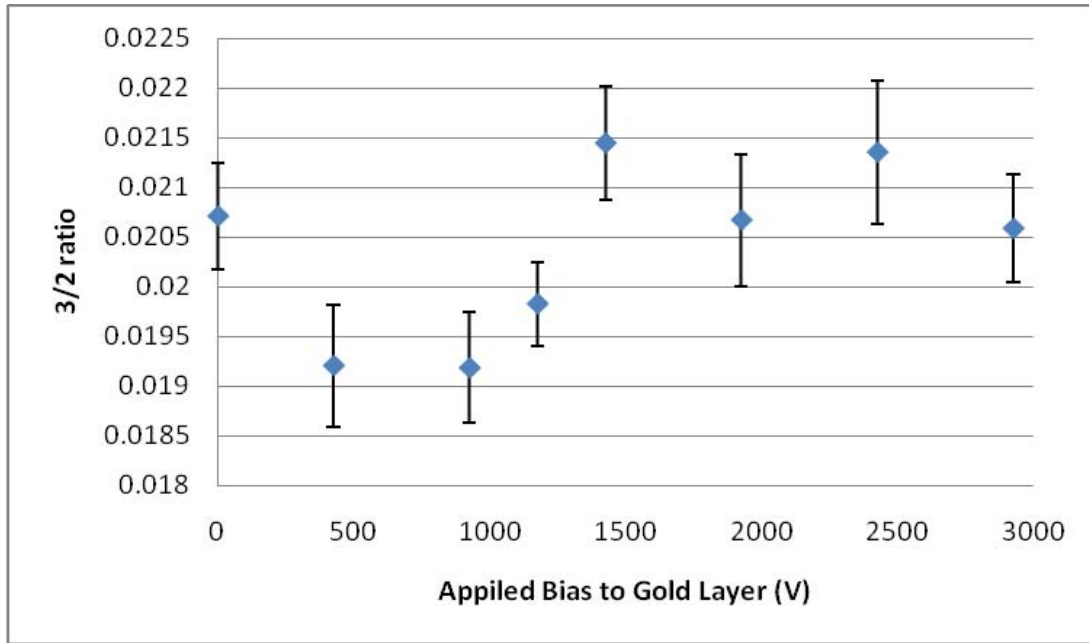


Figure 39. $3\gamma/2\gamma$ ratio results by applying a voltage bias on the inner silver layer and outer gold layer of the capillary tube. The inner bias was adjusted so that the voltage drop from the silver to gold layer was always 75 V. The grounds were both established at the vacuum chamber wall.

The graph indicates that as the two biases are increased, the $3\gamma/2\gamma$ ratio decreases, then starts to rise and remains fairly constant. It appears that the outer, polarizing, electric field is influencing the positrons before Ps is formed. The $3\gamma/2\gamma$ ratio decreases because the outer electric field is increasing the energy of the positron, pushing it above the Ore gap. As the outer bias is increased, the field imparts so much energy to the positrons that they are ejected from the capillary tube. As before, when they annihilate, because the annihilations are off center, the 2γ photons are mistaken for 3γ photons, and incorrectly increase the $3\gamma/2\gamma$ ratio. In addition, the belief that the positrons are being ejected from the capillary tube is supported by the fact that the $3\gamma/2\gamma$ ratio gradually increases as the annihilation occurs more off-center. If the rise in the $3\gamma/2\gamma$ ratio was due to a change in lifetime, the ratio jump would occur suddenly, and not gradually. This conclusion can be confirmed by collecting and analyzing lifetime spectra from the capillary tube.

4.4 PALS Analysis

Due to the poor counting statistics achieved by Lt Slaughter, questions arose as to whether the digital PALS system was working correctly. To test this, a Na-22 source was measured for 1200 sec using the DigitalPALS_1.9.ipf code, and then analyzed using the DigitalPALSTools_1.3.ipf code. The refined data was sent to Dr. Lindsay, and he determined that the system was functioning correctly. The AFIT PALS system was then updated using new code provided by Dr. Lindsay. However, after the newer versions of the PALS codes were updated with the parameters for the AFIT BaF₂ detectors, the system no longer worked properly.

Each time the PALS code was executed, the Igor Pro program froze. All of the previous versions of the PALS code were tested as well, but they too froze up. Next, the oscilloscope was restored to its default settings, but the PALS program continued to freeze. The Igor Pro program was then uninstalled and reinstalled to the oscilloscope, but that did not work. After that, the entire PALS system was loaded onto a different oscilloscope, of the same model, but the program still did not run. After months of unsuccessfully trying to correct the problem, no solution was found. To be able to conduct the lifetime analysis, a system used to conduct positron spectroscopy was altered to measure lifetimes.

The MATLAB™ PALS program proved to have problems as well. Two main problems existed with the MATLAB™ program: calibration and activity. When measuring the standard Sr-85, Co-57, and Cs-137 sources, the energy spectra produced were horrible. As can be seen in Figure 25, identifying the 662 keV peak in the Cs-137

spectra is very difficult. In the spectra from the other sources, it was even harder to identify to the locations of the FEP's. Due to the difficulty in locating the energy peaks in the spectra, large errors were associated with the energy calibrations of the detectors. To fix the problem, the 1,274 and 511 keV trigger voltages were used instead of energy calibrations to run the code. The second problem encountered occurred due to the low activity of the source. The oscilloscope was originally set up so that it would only trigger off of a 1274 keV photon followed by a 511 keV photon. Due to the low activity of the capillary tube, if no pulses met these conditions within a specified amount of time, the system timed out. To fix the problem, the timeout was increased to 60 sec.

Even after fixing the timeout problem, the efficiency of the system was still poor. Although a direct comparison between the PsARS and PALS results could no longer be made, the first capillary tube with the second capillary tube. The specific results are discussed in the next section, but the second capillary tube did have a higher activity than the first capillary tube. Also, to increase the chance of seeing the o-Ps in the lifetime spectrum, the lifetime measurement was conducted with a bias of 75 V applied to the silver layer of the capillary tube. After collecting data for approximately 42 hours, the following results were obtained:

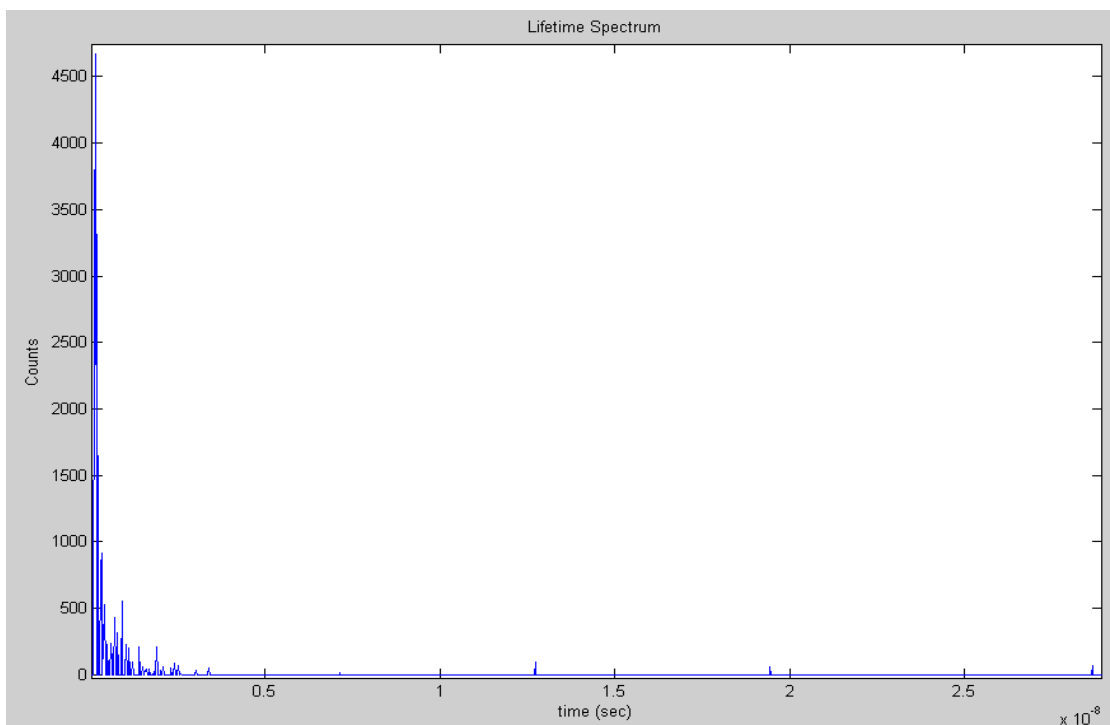


Figure 40. Lifetime spectrum from measuring the second capillary tube, with a bias of 75 V added to the silver layer, for 42 hours.

As can be seen from the spectrum, the system is very inefficient and did not collect enough counts to run a PALSfit analysis. However, the results show that the system is working properly. As expected, most of the counts are in the pico second region due to the annihilation of p-Ps, but peaks from the o-Ps can be seen starting to form. 4 peaks above 5 ns are forming due to the longer lived lifetimes of the o-Ps. These occur at approximately 7 ns, 13 ns, 19 ns, and 29 ns. These longer lifetimes result from the positrons forming o-Ps at the surface of the gold capillary tube. Together with rise in $3\gamma/2\gamma$ ratio, both results proved that at the capillary tube surface, both the $3\gamma/2\gamma$ ratio and positron lifetimes increased. To achieve a spectrum that can be analyzed with PALSfit and to better see the longer lived o-Ps, more counts must be recorded to achieve the required 1 million.

4.5 Second Capillary Tube

0.3 μCi of radioactive Na-22 was intended to be deposited inside the capillary tube. However, problems arose due to the volume of solution needed to deposit the required amount of Na-22 inside the capillary tube. When the first capillary tube was created, approximately 60 μL of the radioactive solution was needed to deposit 0.3 μCi of Na-22 inside the tube. However, due to radioactive decay, this year 85 μL was needed to deposit the same amount of Na-22 inside the capillary tube. The capillary tube was not able to hold the increased volume of liquid and some liquid leaked out the end of the tube. Furthermore, the activity was concentrated on one side of the tube. To counteract these problems in the future, two modifications may be made. The first, the same Na-22 solution can be used, but part of the water must be evaporated to concentrate the Na-22. A second option is to use the other Na-22 solution at AFIT that has a higher activity. After measuring the second capillary tube and comparing its results to those of the first capillary tube, approximately 0.424 μCi of Na-22 (7 Jan 2011) was deposited into the second capillary tube. More than 0.3 μCi of Na-22 was deposited into the capillary tube due to the precision with drawing 85 μL into the syringe. However, the result shows that heating the capillary tube on both sides at a lower temperature prevents pressure from building up inside that would have ejected the solution out.

4.6 Future Improvements

Although many problems with the PsARS system were solved from the previous year, many more still exist. The problem with the vacuum pressure that Lt Slaughter encountered was not resolved. In fact, the problem got worse. While Lt Slaughter was

able to achieve pressures of 10^{-3} torr, this year only pressures of 1.36×10^{-2} torr were achieved. After turning on the roughing pump, initially the vacuum pressure dropped to around 1.07×10^{-3} torr, but then over time the pressure increased to 1.36×10^{-2} torr. To correct the problem, all of the metal gaskets in between the CF flanges were exchanged for new ones, and all of the bolts were tightened around the flanges until the metal gaskets could no longer be seen in between the flanges. In addition, vacuum grease was added to the rubber o-rings in the Klein flanges (KF). For future experiments, all of metal gaskets should be replaced again and the o-rings should be replaced with new rings. Furthermore, the full power of the roughing pump and sensitivity of the sensor needs to be tested because after attaching the vacuum sensor directly to the flange on the pump, the vacuum pressure only reached approximately 1×10^{-2} torr.

The next problem encountered was when the XIA cards would record differing number of events. Even though the two modules would sync up at the beginning of a run, eventually one module would record an event that the other missed. This problem was discussed with the manufacturer of the cards and they determined the problem to exist within the DGF4C's firmware. Unfortunately, the firmware was not able to be updated, but the problem was compensated for in the analysis code. In this experiment, the problem was minimized due to the low activity of the source, but in future experiments, if the activity is increased, the problem will worsen. The best solution to fix the problem would be to buy a new digitizing card with more than four channels on it. A new card will have the updated firmware, and with more than four channels on the card, the process of getting multiple cards to communicate with each other is eliminated.

The next improvement is to increase the efficiency of the analysis code and decrease the runtime of the experiments. In the analysis code, only events with two and three hits were analyzed. Events with three, four, five, or six hits could contain 2γ or 3γ photons with background hits, but these cases were ignored. To make the correction, the code would have to look for 2γ photons in events with three, four, five, and six hits and 3γ photons in events with four, five, and six hits. However, by looking at how many events in a measurement contain five or six hits, the determination can be made to ignore those events if the chance of seeing one is sufficiently low.

A fourth improvement can be made by correcting the problem from having to delete the module information at the top and middle of all of the Igor Pro output files. Currently, the only way to solve the problem is to open up the output file and delete the information by hand. Larger file sizes take longer to load, and once the files become too large, they will not open. The problem can be corrected for either in the PsARS $3\gamma/2\gamma$ code or the Igor Pro program. First, the $3\gamma/2\gamma$ code can be modified to account for the extra information and pass over it as the code scans the data. Secondly, the Igor Pro settings could possibly be changed using the GUI to prevent the output file from having the extra information. If the second solution was chosen and the activity of the source being measured was changed, the timing information on the modules would have to be checked first to ensure the modules are start up simultaneously.

The last problem with the PsARS system occurred due to the difference in dead time for the NaI(Tl) and BaF₂ detectors. The NaI(Tl) needs to measure low activity sources while the BaF₂ detectors need to measure high activity sources to prevent the PALS measurements from taking a week to conduct. To prevent this problem in the

future, independent experiments can be run with different activity sources. Although the two results will not be able to be directly compared to each other, they will still provide useful information about the formation and lifetime of Ps.

The biggest problem encountered with the PALS system came from how the oscilloscope digitized the data. The digitizing rate was too low and the rounding errors within the program became significant. This caused the lifetime spectra to consist on dirac functions. To improve the system, an interpolation technique needs to be added to the MATLAB[™] PALS code when searching for the midrise points of the start and stop pulses. This will reduce the rounding error and improve the timing resolution.

The other major problem with the PALS system was its efficiency. Besides measuring a separate, higher activity source, changes to the code need to be made to adjust the start and stop modules. With only one detector acting as the start module, immediately the efficiency of the system is cut in half. By modifying to the code for both detectors to act as the start modules, the efficiency of the system would double.

Future research on the capillary tube could include having the positron interact with different materials. This can be done in one of two ways. The first would be to deposit another material on the outside of the gold layer. By placing a positive bias on the silver layer, the positrons would be drawn to the gold surface, and with enough energy, escape from the gold layer into new material. With the PALS system, lifetime analysis could be used to characterize the size of the pores in the material. A second experiment would involve filling the vacuum chamber with a gas. Once at the surface of the capillary tube, the positrons would interact with the atoms or molecules in the gas.

5. Conclusion

A new $3\gamma/2\gamma$ code was developed that combined the advantages of using both energy and geometry filters. These changes increased the efficiency and decreased the runtime of the system, allowing for practical measurements to be conducted on low activity sources. The method was calibrated by measuring a copper standard source with a known $3\gamma/2\gamma$ ratio. The source was made by depositing a radioactive $^{22}\text{NaCl}$ solution onto a copper sample and evaporating the water. In previous measurements problems arose due to the capillary bending under the force of gravity. This problem was fixed by designing a ring of polymer that was placed inside the vacuum chamber to hold the free end of capillary tube and keep it centered. In addition, a second capillary tube was created by depositing the radioactive NaCl solution within the tube. The tube was heated on both sides, which prevented a pressure buildup inside the tube that kept the solution inside.

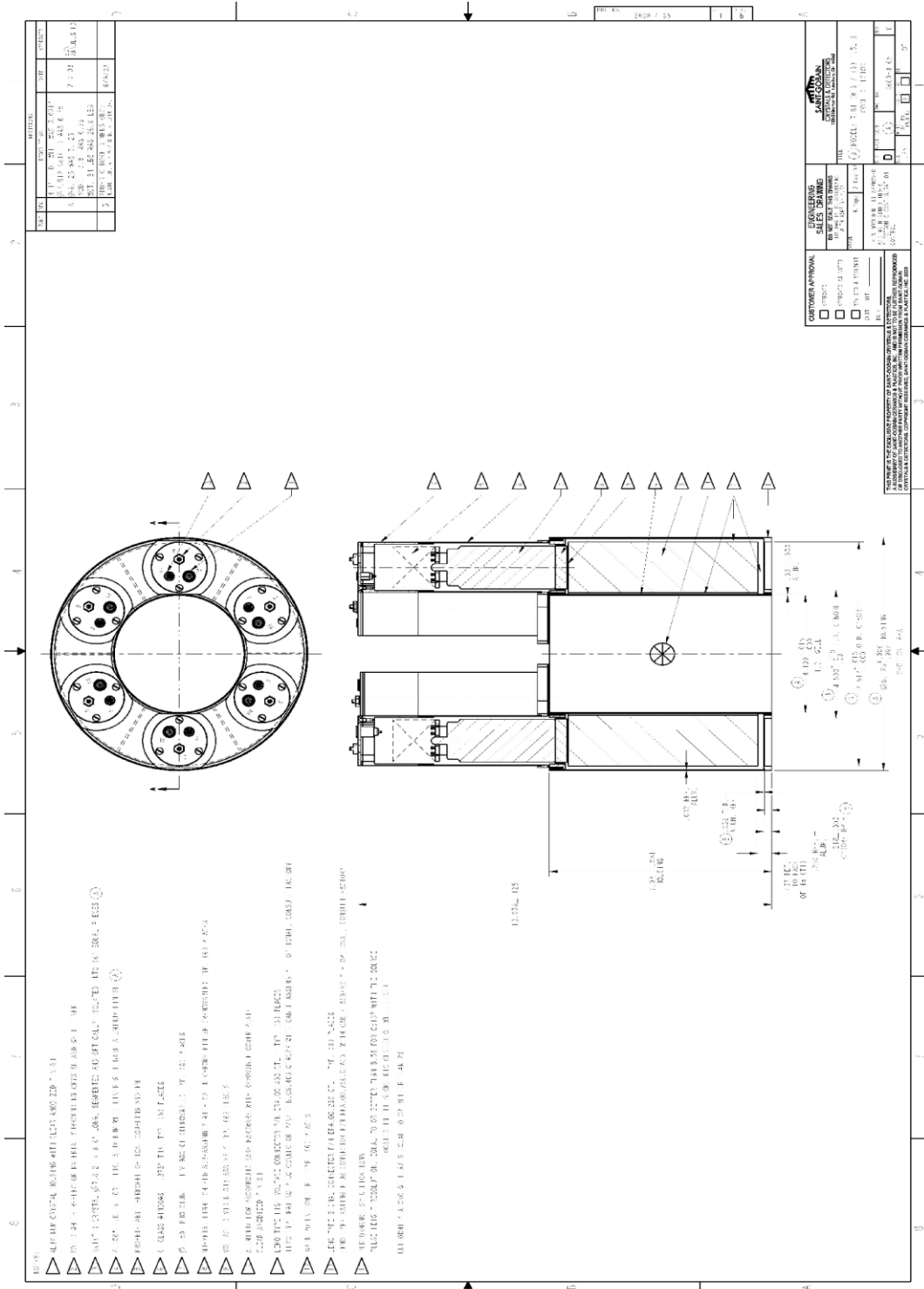
The $3\gamma/2\gamma$ analysis of the capillary tube showed that the inner electric field effectively drew the positrons to the surface of the capillary tube. Once at the surface, they formed Ps. With a bias applied to the silver layer, the $3\gamma/2\gamma$ ratio increased from 0.0186, with no applied field, to 0.0208, with a 75 V bias on the silver layer. Next, the bias on both the silver and gold layer was increased simultaneously, but the voltage drop between the two remained at 75 V. The first electric was supposed to bring the positrons to the surface of the capillary tube and the second field was supposed to polarize the Ps, increasing their annihilation lifetimes. However, the results showed that the second

electric field did not polarize the Ps, but rather forced the positrons to be ejected from the capillary before they could form Ps.

After unsuccessfully troubleshooting the digital PALS system, a second system was developed, the MATLAB™ PALS system. This system was used to measure the second capillary tube with an inner applied bias of 75 V. Even though enough counts were not collected to run a PALSfit analysis, the results showed that the new system works and that forcing the positrons to the surface of the gold layer increased their lifetimes.

This research lead to the development of a new PALS system and a more efficient PsARS system. Together, the results from both systems show that by establishing an electric field across the capillary tube wall would force the positrons to drop into the Ore gap as they reached the surface. In addition, the results proved that at the capillary tube surface both the $3\gamma/2\gamma$ ratio and lifetimes increased. Further research should focus on improving the efficiency of both systems and either adding new materials to the capillary tube or filling the vacuum chamber with different gases and using the positrons to characterize the materials. This research provided the foundation for a new PALS system and led to the development of conducting PsARS measurements in a practical amount of time.

Appendix A. Schematic of NaI(Tl) Ring Detector



Appendix B. MATLAB™ 3 γ /2 γ Analysis Code

```
%program determines the number of 3 and 2 gamma counts

%save data as .dat file in folder, drag the file to the workspace and
%use the import function to load data
data = A15min1250V1175V;
[row,colm]=size(data);

%initialize variables to keep track of the number of each type of count
count2=0;
count3_120=0;
count3_adj=0;
count3_2=0;

%Becuae sometimes each module will end up will different event
numbers,
%this will search for the smaller event number.
%Find the number of events in the 2nd module
event2=data(row,1);
%find the number of events in 1st module
event1=1;
for i=1:(row/2)+10
    if event1<data(i,1)
        event1=data(i,1);
    end
end
%check to see which number of events is less
if event1<event2
    event=event1;
else
    event=event2;
end

%add in energy calibrations
for i=1:event
    %calibrate module 1 ch 1 and 2
    data(4*i-2,3)=(-2.04812e-7*data(4*i-2,3)^2)+(5.21453e-2*data(4*i-
2,3));
    data(4*i-1,3)=(2.43024e-7*data(4*i-1,3)^2)+(1.98521e-2*data(4*i-
1,3));
    %calibrate module 2 ch 0,1,2 and 3
    data(4*event+((i-1)*4)+1,3)=(-3.31639e-8*data(4*event+((i-
1)*4)+1,3)...
        ^2)+(4.80379e-2* data(4*event+((i-1)*4)+1,3));
    data(4*event+((i-1)*4)+2,3)=(2.06727e-7*data(4*event+((i-
1)*4)+2,3)...
        ^2)+(3.37157e-2*data(4*event+((i-1)*4)+2,3));
    data(4*event+((i-1)*4)+3,3)=(3.58532e-7*data(4*event+((i-
1)*4)+3,3)...
        ^2)+(1.52752e-2*data(4*event+((i-1)*4)+3,3));
    data(4*event+((i-1)*4)+4,3)=(-9.97343e-8*data(4*event+((i-
1)*4)+4,3)...
        ^2)+(3.32537e-2*data(4*event+((i-1)*4)+4,3));
```

```

end

for i=1:event

    %check to see if all the times for the events match up
    k=0; %use k to keep track of time matches
    if (data(4*i-3,4)==data(4*i-2,4)) && (data(4*i-3,4)==data(4*i-
1,4)) ...
        && (data(4*i-3,4)==data(4*i,4)) && ...
        (data(4*i-3,4)==data(4*event+((i-1)*4)+1,4)) && ...
        (data(4*i-3,4)==data(4*event+((i-1)*4)+2,4)) && ...
        (data(4*i-3,4)==data(4*event+((i-1)*4)+3,4)) && ...
        (data(4*i-3,4)==data(4*event+((i-1)*4)+4,4))
        k=i;
    else
        for j=i-20:i+20
            if ((j>0) && (j<=event2))
                if data(4*i-2,4)==data(4*event+((j-1)*4)+1,4)
                    %if times don't match up, find the event with the
matching
                    %time. check that all 6 times match because sometimes
the
                    %times change within the event, even when the events
and
                    %times match up
                    if (data(4*i-2,4)==data(4*i-1,4)) && ...
                        (data(4*i-2,4)==data(4*event+((j-
1)*4)+1,4)) ...
                        && (data(4*i-2,4)==data(4*event+((j-
1)*4)+2,4)) ...
                        && (data(4*i-2,4)==data(4*event+((j-
1)*4)+3,4)) ...
                        && (data(4*i-2,4)==data(4*event+((j-
1)*4)+4,4))
                            k=j;
                        end
                    end
                end
            end
        end
    end

    %if program could get the time from mod1 to match to mod2 for an
event,
    %continue on and look for coincidence
    if k>0
        %rename the PMT's to make coding easier to read and write
        %PMT 1 is "A", PMT 2 is "B"...
        A=data(4*i-2,3);
        B=data(4*event+((k-1)*4)+1,3);
        C=data(4*event+((k-1)*4)+2,3);
        D=data(4*i-1,3);
        E=data(4*event+((k-1)*4)+3,3);
        F=data(4*event+((k-1)*4)+4,3);
    end
end

```

```

%check the number of hits for each event
hit=0;
for j=4*i-2:4*i-1
    if data(j,3)>0
        hit=hit+1;
    end
end
for j=4*event+((k-1)*4)+1:4*event+((k-1)*4)+4
    if data(j,3)>0
        hit=hit+1;
    end
end

%check to see if 2 hits are 2gamma or 3gamma count
if hit==2
    sum=0;
    %check if hits are on opposite PMT's for 2gamma count
    if ((A>400)&&(D>400)) && ((A<600)&&(D<600))
        sum= A + D;
    elseif ((B>400)&&(E>400)) && ((B<600)&&(E<600))
        sum= B + E;
    elseif ((C>400)&&(F>400)) && ((C<600)&&(F<600))
        sum3= C + F;
    end
    %if hits are 2 511's, count as a 2 gamma hit(resolution at
    % 511 is 10%, 150 is 20%)
    if ((sum>580) && (sum<1124))
        count2=count2+1;
    end

    %check 3gamma non-adjacent hits ( resolution at 380 is 12%)
    if ((A && C)>50) && ((A && C)<425))
        sum= A + C;
    elseif ((B && D)>50) && ((B && D)<425))
        sum= B + D;
    elseif ((C && E)>50) && ((C && E)<425))
        sum= C + E;
    elseif ((D && F)>50) && ((D && F)<425))
        sum= D + F;
    elseif ((E && A)>50) && ((E && A)<425))
        sum= E + A;
    elseif ((F && B)>50) && ((F && B)<425))
        sum= F + B;
    end
    if ((sum>160) && (sum<850)) % resolution at 380 at 12%,
    % 150+50 is 20%
        count3_2=count3_2+1;
    end
end

%check for 3 hits
if hit==3
    sum=0;

```

```

%check for 120 degree hits (every other detector) (380 at
12%)
    if ((A>50)&&(C>50)&&(E>50)) && ((A<425)&&(C<425)&&
(E<425))
        sum= A + C + E;
    elseif((B>50)&&(D>50)&&(F>50)) && ((B<425)&&
(D<425)&&(F<25))
        sum= B + D + F;
    end
    if ((sum>640) && (sum<1124)) % 340+340 at 12% +50 at 20%
        count3_120=count3_120+1;
    end
%check for opposing hits with an adajecent hit, 380 at 12%)
    if ( ((A && D)&&( C | E ) )>50) && ((A && C && D &&
E)<425))
        sum= A + E + D + C;
    elseif ( ((B && E)&&( D | F ) )>50)&&((B && E && D &&
F)<425))
        sum= B + D + E + F;
    elseif ( ((C && F)&&( E | A ) )>50)&&((A && C && F &&
E)<425))
        sum= C + E + F + A;
    elseif ( ((D && A)&&( F | B ) )>50)&&((A && F && D &&
B)<425))
        sum= D + F + A + B;
    elseif ( ((E && B)&&( A | C ) )>50)&&((A && C && B &&
E)<425))
        sum= E + A + B + C;
    elseif ( ((F && C)&&( B | D ) )>50)&&((F && C && D &&
B)<425))
        sum= F + B + C + D;
    end
    if ((sum>308) && (sum<1124)) % 150+150+50 at 12%
        count3_adj=count3_adj+1;
    end
end
end
end

count2
count3Tot=count3_120+count3_adj+count3_2

```

Appendix C. data_cal_stream.m File

```
% Create a TCPIP interface and device object - Works with 4 Channels
clc
clear all
close all
Run_Start_time = fix(clock) % get time for starting acquisition
dpo.InputBufferSize = 300000; %buffer size
dpo = instrfind('Type', 'tcpip', 'RemoteHost', '169.254.235.51',
'RemotePort', 4000, 'Tag', ''); %Identifies object connecting to

if isempty(dpo)
    dpo = tcpip('169.254.235.51', 4000); % ip address of DPO7104
else
    fclose(dpo);
    dpo = dpo(1);
end

deviceObj = icdevice('tektronix_dpo7104_r1.mdd', dpo); %Connecting to
scope using driver called tektronix_dpo_7104_r1.mdd

%Connect to the scope
connect(deviceObj);
%% Scope Settings
fprintf(dpo, 'Select:Ch3 On') % turns input for channel 3 on
fprintf(dpo, 'Select:Ch4 On') % turns input for channel 4 on
fprintf(dpo, 'CH3:Position 0') % Aligns channel 3 at 0 V
fprintf(dpo, 'CH4:Position 0') % Aligns channel 4 at 0 V
fprintf(dpo, 'Horizontal:Position 20') % Places signals at designated
horizontal location (10)
fprintf(dpo, 'ch3:Scale .04'); % Sets vertical scale for channel 3
(V/div)
fprintf(dpo, 'ch4:Scale .04'); % Sets vertical scale for channel 4
(V/div)
% Trigger Setting
fprintf(dpo, 'Trigger:Enhance Off'); % Toggles enhanced triggering mode
fprintf(dpo, 'Trigger:A:Type Logic'); % Sets the A trigger mode as a
Logic
fprintf(dpo, 'Trigger:A:Logic:Class Pattern'); % Sets the A trigger to
use the Pattern Mode
fprintf(dpo, 'Trigger:A:Logic:Function And'); % {AND|NANd|NOR|OR} Sets
boolean logic to perform on triggered events
% AND specifies to trigger if all conditions are true.
% NANd specifies to trigger if any of the conditions are false.
% NOR specifies to trigger if all conditions are false.
% OR specifies to trigger if any of the conditions are true.
fprintf(dpo, 'Trigger:A:Logic:Pattern:Input:CH3 High'); % {HIGH|LOW|X}
Sets importance level for channel 1 (High)
fprintf(dpo, 'Trigger:A:Logic:Pattern:Input:CH4 High'); % Sets
importance level for channel 2 (High)
fprintf(dpo, 'Trigger:A:Logic:Input:Format Binary'); % Sets data format
to Binary Can also be 'Hexadecimal'
fprintf(dpo, 'Trigger:A:Logic:Pattern:When False'); %
{TRUE|FALSE|LESSThan|MOREThan} Sets condition for meeting boolean logic
```

```

fprintf(dpo, 'Trigger:A:Logic:Threshold:CH3 -.01'); % Sets trigger level
for Channel 3
fprintf(dpo, 'Trigger:A:Logic:Threshold:CH4 -.01'); % Sets trigger level
for Channel 4
fprintf(dpo, 'Trigger:A:Mode Normal'); % Sets trigger mode to Normal
(Other option is Auto -> forces trigger at timeout period)
fprintf(dpo, 'ACQUIRE:MODE HiRes'); %Sets sampling mode to High
Resolution Mode

NumberOfPoints = str2num(query(dpo, 'HORIZONTAL:MODE:RECORDLENGTH?')); %
Queries the record length (number of points per waveform)
SampleRate = str2num(query(dpo, 'HORIZONTAL:MODE:SAMPLERATE?')); %
Queries the sample rate of the scope
TimeSpan = NumberOfPoints/SampleRate; % Returns seconds per point
timearray = linspace(0,TimeSpan,NumberOfPoints); % Array of time

fprintf(dpo, 'Data:Encdg Ribinary'); % Specifies signed integer-data
point representation with the most significant byte transferred first
(Try SIRBINARY)
fprintf(dpo, 'WFMOutpre:BYT_NR 2'); % Sets the binary width of the data
fprintf(dpo, 'DATA:START 200'); % Sets the beginning of the waveform
data to transfer
fprintf(dpo, 'DATA:STOP 1450'); % Sets the end of the waveform data to
transfer
fprintf(dpo, 'WFMOutpre:ENCDG BIN') % Sets incoming data to binary
format
fprintf(dpo, 'WFMInpre:ENCDG BINARY') % Sets outgoing data to binary
format (Lose?)
fprintf(dpo, 'WFMInpre:BN_FMT RI'); % Specifiies integer-data point
representaoitn (Lose?)
fprintf(dpo, 'WFMInpre:BYT_NR 2');%set 2 byte format = int16 (Lose?)
fprintf(dpo, 'Horizontal:FastFrame:State 0');
fprintf(dpo, 'DATA:SOURCE Ch3'); % Sets data source to Channel 3
Ch3Ymult = str2num(query(dpo, 'WFMOutpre:YMult?')); % Returns vertical
scale factor
Ch3Yoff = str2num(query(dpo, 'WFMOutpre:Yzero?')); % Returns the offset
factor
fprintf(dpo, 'DATA:SOURCE Ch4'); % Sets data source to Channel 4
Ch4Ymult = str2num(query(dpo, 'WFMOutpre:YMult?')); % Returns vertical
scale factor
Ch4Yoff = str2num(query(dpo, 'WFMOutpre:Yzero?')); % Returns the offset
factor

fprintf(dpo, 'DATA:SOURCE Ch3,CH4'); % Reinitiates data source to all
channels
nSamples=5500000; % Sets the number of sammples to acquire (set really
large to allow for time acquisition instead of number of acquisitions)
minutes_run = 1; % Sets how many minutes to acuire data for
seconds_run = minutes_run*60; % Changes length of acquisition to
seconds
tstart = tic; % Start acquisition timer
for i = 1:nSamples
    fprintf(dpo, 'CURVE?'); % Call waveform (writes out in list mode
Channel 1 first then Channel2 then...)

```

```

        Channel(:,1) = Ch3Ymult*binblockread(dpo, 'int16')+Ch3Yoff; % Reads
Channel 3 and scales it
        Channel(:,2) = Ch4Ymult*binblockread(dpo, 'int16')+Ch4Yoff; % Reads
Channel 4 and scales it
        fprintf(dpo, '*wai'); % Makes scope wait to finish tranfer before
executing next command
        fread(dpo,1); % Clears extra terminator from 'CURVE?' cmd
        fprintf(dpo, '*wai'); % Makes scope wait to finish tranfer before
executing next command
        if i==1
            save('Na22_Spec2.txt','Channel','-ascii','-tabs')
        else
            save('Na22_Spec2.txt','Channel','-append','-ascii','-tabs')
        end
        if toc(tstart) > seconds_run % Exit for loop when timing criteria
has been met
            break
        end
    end
end
Sample_Collection_Time = toc(tstart) % Gives how long acquisition took
Run_Stop_time = fix(clock) % Gives current time

```

Appendix D. cal_scan.m File

```
close all
clear all
clc
Run_Start_time = fix(clock)
clear segarray;
NumberOfPoints = 1251;
block_size = NumberOfPoints*100; %must match the number of points per
waveform you transmitt

% describe the format of the data
% for more information, see the textscan reference page
file_id = fopen('Na22_Spec.txt'); %establish ID for file you open up

count = 0;
channel3= [];
channel4 = [];
while ~feof(file_id) %runs to end of file
    count = count+1;
    segarray = textscan(file_id,'%n%n',block_size,'delimiter','');
%reads in a block of data
    [channel3_new,channel4_new] = cal_func(segarray,NumberOfPoints);
    channel3 = [channel3; channel3_new];
    channel4 = [channel4; channel4_new];
end

fclose(file_id);

[channel3_ph,xoutch3]=hist(channel3(:,1),1024);
[channel4_ph,xoutch4]=hist(channel4(:,1),1024);

figure(1)
plot(xoutch3,channel3_ph)
title('ch3')

figure(2)
plot(xoutch4,channel4_ph)
title('ch4')

Run_Stop_time = fix(clock)
```


Appendix E. cal_func.m Function File

```
function [channel3_out,channel4_out] =  
cal_func(segarray,NumberOfPoints)  
Channel3 = cell2mat(segarray(:,1));  
Channel3 = reshape(Channel3,NumberOfPoints,[]);  
  
Channel4 = cell2mat(segarray(:,2));  
Channel4 = reshape(Channel4,NumberOfPoints,[]);  
  
clear segarray  
SampleRate = 1.0000e+009; % Sample rate of scope  
TimeSpan = NumberOfPoints/SampleRate; % Returns seconds per point  
timearray = linspace(0,TimeSpan,NumberOfPoints); % Array of time  
detnum=2; % Number of detectors  
trigger_level = 10e-3; % Trigger level in V, must be above noise  
[num_points,num_wfms] = size(Channel3); % Determines how many waveforms  
were recorded  
  
Channel3filt = sgolayfilt(Channel3,9,13);  
Channel4filt = sgolayfilt(Channel4,9,13);  
  
clear Channel3  
clear Channel4  
  
[pulse_peak_ch3,min_index_ch3] = min(Channel3filt); % Find the pulse  
height of each pulse and the index of that pulse height for channel 3  
[pulse_peak_ch4,min_index_ch4] = min(Channel4filt); % Find the pulse  
height of each pulse and the index of that pulse height for channel 4  
  
midrise_time_ch3 = zeros(1,num_wfms);  
midrise_time_ch4 = zeros(1,num_wfms);  
pulse_order_time_comp = zeros(num_wfms,2);  
pulse_order_index = zeros(num_wfms,2);  
energy_order_index = zeros(num_wfms,2);  
  
% for i = 1:num_wfms  
%  
[midrise_time_ch1(i)]=find_midrise_time(Channel1filt(:,i),timearray,tri  
gger_level); % Calls function "find_trigger_time" and gives the timing  
for each triggered event for Channel 3 (time is off of the trigger)  
%  
[midrise_time_ch2(i)]=find_midrise_time(Channel2filt(:,i),timearray,tri  
gger_level); % Calls function "find_trigger_time" and gives the timing  
for each triggered event for Channel 4 (time is off of the trigger)  
% end  
  
pulse_peak_ch3 = -pulse_peak_ch3; % Changes pulse values from negative  
to positive for channel 3  
en_cal_ch3 = pulse_peak_ch3;  
pulse_peak_ch4 = -pulse_peak_ch4; % Changes pulse values from negative  
to positive for channel 4  
en_cal_ch4 = pulse_peak_ch4;
```

```

for j = 1:num_wfms
    if en_cal_ch3(j) < trigger_level % If waveform peak is below
trigger level then call it a NaN
        en_cal_ch3(j) = NaN; % If waveform peak is below trigger level
then call it a NaN
    end
    if en_cal_ch4(j) < trigger_level % If waveform peak is below
trigger level then call it a NaN
        en_cal_ch4(j) = NaN; % If waveform peak is below trigger level
then call it a NaN
    end
end
[ch3row,ch3col] = size(en_cal_ch3);
[ch4row,ch4col] = size(en_cal_ch4);
if ch3col>0
    channel3_out = en_cal_ch3';
else
    channel3_out = [];
end

if ch4col>0
    channel4_out = en_cal_ch4';
else
    channel4_out = [];
end

end

```

Appendix F. Stream_data_PALS.m File

```
% Create a TCPIP interface and device object - Works with 4 Channels
clc
clear all
close all
Run_Start_time = fix(clock) % get time for starting acquisition
dpo.InputBufferSize = 3000000; %buffer size
dpo = instrfind('Type', 'tcpip', 'RemoteHost', '169.254.235.51',
'RemotePort', 4000, 'Tag', ''); %Identifies object connecting to

if isempty(dpo)
    dpo = tcpip('169.254.235.51', 4000); % ip address of DPO7104
else
    fclose(dpo);
    dpo = dpo(1);
end

deviceObj = icdevice('tektronix_dpo7104_r1.mdd', dpo); %Connecting to
scope using driver called tektronix_dpo_7104_r1.mdd

%Connect to the scope
connect(deviceObj);
dpo.Timeout = 60;
%% Scope Settings
fprintf(dpo, 'Select:Ch3 On') % turns input for channel 3 on
fprintf(dpo, 'Select:Ch4 On') % turns input for channel 4 on
fprintf(dpo, 'CH3:Position 0') % Aligns channel 3 at 0 V
fprintf(dpo, 'CH4:Position 0') % Aligns channel 4 at 0 V
fprintf(dpo, 'Horizontal:Position 20') % Places signals at designated
horizontal location (10)
fprintf(dpo, 'ch3:Scale .05'); % Sets vertical scale for channel 3
(V/div)
fprintf(dpo, 'ch4:Scale .05'); % Sets vertical scale for channel 4
(V/div)
% Trigger Setting
fprintf(dpo, 'Trigger:Enhance Off'); % Toggles enhanced triggering mode
fprintf(dpo, 'Trigger:A:Type Logic'); % Sets the A trigger mode as a
Logic
fprintf(dpo, 'TRIGger:A:LOGic:SETHold:CLOCK:EDGE FALL');
fprintf(dpo, 'TRIGger:A:LOGic:SETHold:CLOCK:SOURce CH3');
fprintf(dpo, 'TRIGGER:A:LOGIC:SETHOLD:CLOCK:THRESHOLD:Ch3 -0.06');
fprintf(dpo, 'TRIGGER:A:LOGIC:SETHOLD:DATA:SOURCE CH4');
fprintf(dpo, 'TRIGGER:A:LOGIC:SETHOLD:DATA:THRESHOLD:CH4 -0.01');
fprintf(dpo, 'TRIGGER:A:LOGIC:SETHOLD:HOLDTIME 0.00');
fprintf(dpo, 'TRIGger:A:LOGic:SETHold:QUALify OCCurs');
fprintf(dpo, 'TRIGGER:A:LOGIC:SETHOLD:SETTIME 100E-9');
% fprintf(dpo, 'Trigger:A:Logic:Class Pattern'); % Sets the A trigger
to use the Pattern Mode
% fprintf(dpo, 'Trigger:A:Logic:Function Or')
% fprintf(dpo, 'Trigger:A:Logic:Pattern:Input:CH3 High'); % {HIGH|LOW|X}
Sets importance level for channel 3 (High)
% fprintf(dpo, 'Trigger:A:Logic:Pattern:Input:CH4 High'); % Sets
importance level for channel 4 (High)
```

```

fprintf(dpo, 'Trigger:A:Logic:Input:Format Binary'); % Sets data format
to Binary Can also be 'Hexadecimal'
% fprintf(dpo, 'Trigger:A:Logic:Pattern:When True'); %
{TRUE|FALSE|LESSThan|MOREThan} Sets condition for meeting boolean logic
% fprintf(dpo, 'Trigger:A:Logic:Threshold:CH3 -.095'); % Sets trigger
level for Channel 3
% fprintf(dpo, 'Trigger:A:Logic:Threshold:CH4 -.035'); % Sets trigger
level for Channel 4
fprintf(dpo, 'Trigger:A:Mode Normal'); % Sets trigger mode to Normal
(Other option is Auto -> forces trigger at timeout period)
fprintf(dpo, 'ACQUIRE:MODE HiRes'); %Sets sampling mode to High
Resolution Mode

NumberOfPoints = str2num(query(dpo, 'HORIZONTAL:MODE:RECORDLENGTH?')); %
Queries the record length (number of points per waveform)
SampleRate = str2num(query(dpo, 'HORIZONTAL:MODE:SAMPLERATE?')) %
Queries the sample rate of the scope
TimeSpan = NumberOfPoints/SampleRate; % Returns seconds per point
timearray = linspace(0,TimeSpan,NumberOfPoints); % Array of time

fprintf(dpo, 'Data:Encdg Ribinary'); % Specifies signed integer-data
point representation with the most significant byte transferred first
(Try SIRBINARY)
% fprintf(dpo, 'Data:Width 2');
fprintf(dpo, 'WFMOutpre:BYT_NR 2'); % Sets the binary width of the data
fprintf(dpo, 'DATA:START 200'); % Sets the beginning of the waveform
data to transfer
fprintf(dpo, 'DATA:STOP 700'); % Sets the end of the waveform data to
transfer
fprintf(dpo, 'WFMOutpre:ENCDG BIN') % Sets incoming data to binary
format
fprintf(dpo, 'WFMInpre:ENCDG BINARY') % Sets outgoing data to binary
format (Lose?)
fprintf(dpo, 'WFMInpre:BN_FMT RI'); % Specifies integer-data point
representaoitn (Lose?)
fprintf(dpo, 'WFMInpre:BYT_NR 2'); %set 2 byte format = int16 (Lose?)
fprintf(dpo, 'Horizontal:FastFrame:State 0');
fprintf(dpo, 'DATA:SOURCE Ch3'); % Sets data source to Channel 3
Ch3Ymult = str2num(query(dpo, 'WFMOutpre:YMult?')); % Returns vertical
scale factor
Ch3Yoff = str2num(query(dpo, 'WFMOutpre:Yzero?')); % Returns the offset
factor
fprintf(dpo, 'DATA:SOURCE Ch4'); % Sets data source to Channel 4
Ch4Ymult = str2num(query(dpo, 'WFMOutpre:YMult?')); % Returns vertical
scale factor
Ch4Yoff = str2num(query(dpo, 'WFMOutpre:Yzero?')); % Returns the offset
factor

fprintf(dpo, 'DATA:SOURCE Ch3,CH4'); % Reinitiates data source to all
channels
nSamples=1000000000; % Sets the number of samples to acquire (set
really large to allow for time acquisition instead of number of
acquisitions)
minutes_run = 1440; % Sets how many minutes to acquire data for

```

```

seconds_run = minutes_run*60; % Changes length of acquisition t
o seconds
tstart = tic; % Start acquisition timer
for i = 1:nSamples
    fprintf(dpo, 'CURVE?'); % Call waveform (writes out in list mode
Channel 1 first then Channel2 then...)
    Channel(:,1) = Ch3Ymult*binblockread(dpo, 'int16')+Ch3Yoff; % Reads
Channel 3 and scales it
    Channel(:,2) = Ch4Ymult*binblockread(dpo, 'int16')+Ch4Yoff; % Reads
Channel 4 and scales it
    fprintf(dpo, '*wai'); % Makes scope wait to finish tranfer before
executing next command
    fread(dpo,1); % Clears extra terminator from 'CURVE?' cmd
    fprintf(dpo, '*wai'); % Makes scope wait to finish tranfer before
executing next command

    pulse_peak_ch3 = min(Channel(:,1)); % Find the pulse height of
each pulse for channel 3
    pulse_peak_ch4 = min(Channel(:,2));
    if (pulse_peak_ch3>-.2 && pulse_peak_ch4>-.2)
        if i==1
            save('C75V_Cap2.txt', 'Channel', '-ascii', '-tabs')
        else
            save('C75V_Cap2.txt', 'Channel', '-append', '-ascii', '-tabs')
        end
    end
    if toc(tstart) > seconds_run % Exit for loop when timing criteria
has been met
        break
    end
end
Sample_Collection_Time = toc(tstart) % Gives how long acquisition took
Run_Stop_time = fix(clock) % Gives current time

```

Appendix G. PALS_meas.m File

```
close all
clear all
clc
Run_Start_time = fix(clock)
clear segarray;
NumberOfPoints = 501; %must match the number of points per waveform you
transmitt

block_size = NumberOfPoints*1;

% describe the format of the data
% for more information, see the textscan reference page
file_id = fopen('B75V_Cap2.txt'); %establish ID for file you open up

count = 0;
PALS_time= [];
while ~feof(file_id) %runs to end of file
    count = count+1;
    segarray = textscan(file_id,'%n%n',block_size,'delimiter','');
    %reads in a block of data
    [PALS_time_new] = pals_func(segarray,NumberOfPoints);
    PALS_time = [PALS_time; PALS_time_new];
end

fclose(file_id);

[pals_time,xoutPals]=hist(PALS_time(:,1),1024);

figure()
plot(xoutPals,pals_time)
title('Lifetime Spectrum')
xlabel('time (sec)')
ylabel('Counts')

Run_Stop_time = fix(clock)
```

Appendix H: PALS_func.m File

```
function [PALS_time] = pals_func(segarray,NumberOfPoints)
PALS_time=[];
Channel3 = cell2mat(segarray(:,1));
Channel3 = reshape(Channel3,NumberOfPoints,[]);

Channel4 = cell2mat(segarray(:,2));
Channel4 = reshape(Channel4,NumberOfPoints,[]);

clear segarray
SampleRate = 1.0000e+10; % Sample rate of scope
TimeSpan =NumberOfPoints/SampleRate; % Returns seconds per point
timearray = linspace(0,TimeSpan,NumberOfPoints); % Array of time
detnum=2; % Number of detectors
max_coincidence_window = 100e-9; % Width of coincidence window in
seconds
trigger_level = 10e-3; % Trigger level in V, must be above noise
[num_points,num_wfms] = size(Channel3); % Determines how many waveforms
were recorded

Channel3filt = sgolayfilt(Channel3,9,39);

Channel4filt = sgolayfilt(Channel4,9,39);

[pulse_peak_ch3,min_index_ch3] = min(Channel3filt); % Find the pulse
height of each pulse and the index of that pulse height for channel 3
[pulse_peak_ch4,min_index_ch4] = min(Channel4filt); % Find the pulse
height of each pulse and the index of that pulse height for channel 4

trigger_level_ch3 = .01; %V
trigger_level_ch4 = .01; %V

midrise_time_ch3 = zeros(1,num_wfms);
midrise_time_ch4 = zeros(1,num_wfms);
pulse_order_time_comp = zeros(num_wfms,2);
pulse_order_index = zeros(num_wfms,2);
energy_order_index = zeros(num_wfms,2);

for i = 1:num_wfms

[midrise_time_ch3(i)]=find_midrise_time(Channel3filt(:,i),timearray,tri
gger_level); % Calls function "find_trigger_time" and gives the timing
for each triggered event for Channel 3 (time is off of the trigger)

[midrise_time_ch4(i)]=find_midrise_time(Channel4filt(:,i),timearray,tri
gger_level); % Calls function "find_trigger_time" and gives the timing
for each triggered event for Channel 4 (time is off of the trigger)
end

pulse_peak_ch3 = -pulse_peak_ch3; % Changes pulse values from negative
to positive for channel 3
en_cal_ch3=pulse_peak_ch3;
```

```

pulse_peak_ch4 = -pulse_peak_ch4; % Changes pulse values from negative
to positive for channel 4
en_cal_ch4=pulse_peak_ch4;

for j = 1:num_wfms
    if en_cal_ch3(j) < trigger_level_ch3 % If waveform peak is below
trigger level then call it a NaN
        en_cal_ch3(j) = NaN; % If waveform peak is below trigger level
then call it a NaN
        midrise_time_ch3(j) = NaN; % If waveform peak is below trigger
level then call it a NaN
    end
    if en_cal_ch4(j) < trigger_level_ch4 % If waveform peak is below
trigger level then call it a NaN
        en_cal_ch4(j) = NaN; % If waveform peak is below trigger level
then call it a NaN
        midrise_time_ch4(j) = NaN; % If waveform peak is below trigger
level then call it a NaN
    end

    pulse_order_time_comp(j,1) = midrise_time_ch3(j); % Duplicate
timing values to place in array to sort pulses
    pulse_order_time_comp(j,2) = midrise_time_ch4(j); % Duplicate
timing values to place in array to sort pulses
    lowerbound_511 = .01;
    upperbound_511 = .056;
    lowerbound_1274 = .06;
    upperbound_1274 = .15;
    if ( (midrise_time_ch4(j)-
midrise_time_ch3(j)<max_coincidence_window) && (midrise_time_ch4(j)-
midrise_time_ch3(j)>0) )
        if (en_cal_ch4<upperbound_511 && en_cal_ch4>lowerbound_511) &&
(en_cal_ch3<upperbound_1274 && en_cal_ch3>lowerbound_1274)
            PALS_time(j) = abs(midrise_time_ch3(j)-
midrise_time_ch4(j));
        else
            % PALS_time(j) = [];
        end
    end
end
end
end

```


Appendix I. find_midrise_time.m File

```
%%Find the time for halfway up rise of pulse
function [halfpeak_time] =
find_midrise_time(Channel,timearray,trigger_level)
    if min(Channel) <= -trigger_level
        percent50 = .5*min(Channel);
        midrise = percent50;
        indexabove = find(Channel<midrise,1,'first');
        if indexabove > 1
            indexbelow = indexabove - 1;
        else
            indexbelow = 1;
        end
        abovediff = abs(Channel(indexabove)-midrise);
        belowdiff = abs(Channel(indexbelow)-midrise);
        if abovediff < belowdiff
            halfpeak_time = timearray(indexabove);
        else
            halfpeak_time = timearray(indexbelow);
        end
    else
        halfpeak_time = NaN;
    end
end
```

Bibliography

1. M Charlton and J.W. Humberston. *Positron Physics*. Cambridge University Press, New York, 2005.
2. Slaughter. *Positron Annihilation of Radiation Spectroscopy (PsARS) Applied to Positronium Formation Studies*: AFIT. 2010
3. Y. C. Jean, P.E. Mallon, and D. M. Schrader. *Principles and Applications of Positron and Positronium Chemistry*. World Scientific, New Jersey, 2003.
4. M. M. Nieto, M. H. Holzscheiter, and T. J. Phillips. 2003 *J Opt. B* **5** S547-S552.
5. Y. Ito. 2003 *Radiation Physics and Chemistry*. **68** 403-7.
6. A. Sun, C. Edwards, A. Kane, and S. Pandipati. 1993 *IEEE* November 44-6.
7. Teasdale. *Solid Rocket Microrockets*. UC Berkeley. 2000. <http://www-bsac.eecs.berkeley.edu/projects/microrockets/masters_report.pdf>
8. R. M. Nieinen and J. Oliva 1980 *Phys. Rev. B* **22** 2226-47.
9. D. G. Costello, D.E. Groce, D.F. Herring, and J. Wm. McGowan. 1972. *Phys. Rev. B* **5** 1433-6.
10. S. Mukherjee et all. 2008. *Applied Surface Science*. **255** 223-6.
11. Burggraf, Larry. Professor, AFIT Department of Engineering Physics, WPAFB OH. Personal correspondence. 30 June 2010.
12. R. Krause-Rehberg and H.S. Leipner. *Positron Annihilation in Semiconductors*. Springer, New York, 1999.
13. "Data Acquisition," *Wavemetrics 30 Dec 2010*.
<<http://www.wavemetrics.com/products/igorpro/dataaccess/hardwaredata.htm>>.
14. M. Bertolaccini, C. Bussolati, and L. Zappa. 1965. *Physical Review A*. **139** 696-9.
15. Glenn F. Knoll *Radiation Detection and Measurement*. John Wiley and Sons, Inc, New Jersey, 2000.
16. R. J. Stevens and P.C. Lichtenberger 1972. *Physc. Rev. Lett.*, **29**, 166-9.

17. “Pixie-500,” XIA. 10 Jan 2011. <http://xia.com/DGF_Pixie-500.html>.
18. S. D. Howe and G. A. Smith “Enabling Exploration of Deep Space: High Density Storage of Antimatter”. *Synergistic Technologies, Inc.*
<http://www.niac.usra.edu/files/studies/final_report/24Howe.pdf>.
19. “Positron Lifetime Spectroscopy” *PositronAnnihilation.Net*. 28 Jan 2011.
<http://www.positronannihilation.net/index_files/Positron%20Lifetime%20Spectroscopy.pdf>.
20. Burggraf, Larry. Professor, AFIT Department of Engineering Physics, WPAFB OH. Personal correspondence. 4 November 2010.
21. “DGF4C” XIA. 11 Feb 2011. <http://www.xia.com/Datasheets/DGF_F_flyer.pdf>.
22. S. Szpala et al. 1996. *Physical Review B*. **54** 4722-4731.
23. A. P. Mills Jr., D. B. Cassidy, and R. G. Greaves 2004. *Material Science Forum*. **445-446** 424-9.
24. C. S. Williams et al. 2010. *IEEE*. **75** 860-9.
25. M. H. Weber and K. G. Lynn. 2000. *Radiation Physics and Chemistry*. **58** 749-753.
26. A. Ore and J. L. Powell 1949. *Physical Review*. **75** 1696-9.
27. S. DeBenedetti and R. T. Siegel 1954. *Physical Review*. **94** 955-9.
28. C. H. Hodges and M. J. Scott. 1973. *Physical Review B*. **7** 73-9.
29. T. M. Mayer et al. 1999. *Journal of Applied Physics*. **85** 8170-7.
30. J. V. Olsen, P. Kirkegaard, N. J. Pedersen, and M. Eldrup. 2006. “PALSfit: A computer program for analyzing positron lifetime spectra” *Risø National Laboratory*.

REPORT DOCUMENTATION PAGE				Form Approved OMB No. 074-0188	
<p>The public reporting burden for this collection of information is estimated to average 1 hour per response, including the time for reviewing instructions, searching existing data sources, gathering and maintaining the data needed, and completing and reviewing the collection of information. Send comments regarding this burden estimate or any other aspect of the collection of information, including suggestions for reducing this burden to Department of Defense, Washington Headquarters Services, Directorate for Information Operations and Reports (0704-0188), 1215 Jefferson Davis Highway, Suite 1204, Arlington, VA 22202-4302. Respondents should be aware that notwithstanding any other provision of law, no person shall be subject to a penalty for failing to comply with a collection of information if it does not display a currently valid OMB control number.</p> <p>PLEASE DO NOT RETURN YOUR FORM TO THE ABOVE ADDRESS.</p>					
1. REPORT DATE (DD-MM-YYYY) 24-03-2011		2. REPORT TYPE Master's Thesis		3. DATES COVERED (From - To) July 2010-March 2011	
4. TITLE AND SUBTITLE Positron annihilation ratio spectroscopy study of electric fields applied to positronium at material interfaces				5a. CONTRACT NUMBER	
				5b. GRANT NUMBER	
				5c. PROGRAM ELEMENT NUMBER	
6. AUTHOR(S) Walker, Ariella Courtney 2 nd Lt USAF				5d. PROJECT NUMBER 11P218	
				5e. TASK NUMBER	
				5f. WORK UNIT NUMBER	
7. PERFORMING ORGANIZATION NAME(S) AND ADDRESS(S) Air Force Institute of Technology Graduate School of Engineering and Management (AFIT/EN) 2950 Hobson Way WPAFB OH 45433-7765				8. PERFORMING ORGANIZATION REPORT NUMBER AFIT/GNE/ENP/11-M19	
9. SPONSORING/MONITORING AGENCY NAME(S) AND ADDRESS(ES) Air Force Office of Scientific Research Dr. C Michael Lindsay 2306 Perimeter Rd, Eglin AFB, FL 32542 DSN 872-1543 Dr. Michael R. Berman 801 North Randolph Street, Arlington, VA 22203 Phone: 703 426-7781				10. SPONSOR/MONITOR'S ACRONYM(S) AFOSR	
				11. SPONSOR/MONITOR'S REPORT NUMBER(S)	
12. DISTRIBUTION/AVAILABILITY STATEMENT APPROVED FOR PUBLIC RELEASE; DISTRIBUTION UNLIMITED					
13. SUPPLEMENTARY NOTES					
<p>14. ABSTRACT The purpose of this research was to develop a new code to analyze the data from AFIT's positron annihilation of radiation spectrometer, PsARS, system. The PsARS was used to analyze positronium formation at the surface of a capillary tube coated with gold. Using energy and geometry filters, the PsARS code determined the ratio of ortho-positronium to para-positronium. An electric field applied across the capillary tube wall forced positrons to move towards the gold surface of the capillary tube and prevent them from dropping into the Ore gap before they reach the surface. Inside the Ore gap, the positrons are more likely to form positronium. With the addition of the electric field, the positrons gain energy to overcome the loss of energy from scattering. Once at the surface, a secondary electric field applied from the capillary tube surface to the vacuum chamber wall polarized the positronium, increasing their lifetimes. The capability to force the positrons to gather on the gold surface of the capillary tube was demonstrated. In addition to the PsARS system, a positron annihilation lifetime spectroscopy, PALS, system was used to analyze the lifetimes of the positrons.</p>					
15. SUBJECT TERMS Positron annihilation, ortho-positronium, para-positronium, annihilation lifetime					
16. SECURITY CLASSIFICATION OF:			17. LIMITATION OF ABSTRACT UU	18. NUMBER OF PAGES 116	19a. NAME OF RESPONSIBLE PERSON Larry Burggraf, AFIT ENP
a. REP ORT	b. ABSTRA CT	c. THIS PAGE			19b. TELEPHONE NUMBER (Include area code) 937-255-3636 x4507 Larry.burggraf@afit.edu
U	U	U			